Biochimica et Biophysica Acta 1840 (2014) 2886–2903

Contents lists available at ScienceDirect

Biochimica et Biophysica Acta

journal homepage: www.elsevier.com/locate/bbagen

Synthesis and characterization of 1*H*-phenanthro[9,10-*d*]imidazole derivatives as multifunctional agents for treatment of Alzheimer's disease

Jinggong Liu [a], Jun Qiu [a], Mingxue Wang [a], Ling Wang [a], Lijuan Su [a], Jinbo Gao [b], Qiong Gu [a], Jun Xu [a], Shi-Liang Huang [a], Lian-Quan Gu [a], Zhi-Shu Huang [a,*], Ding Li [a,**]

[a] School of Pharmaceutical Sciences, Sun Yat-sen University, Guangzhou University City, 132 Waihuan East Road, Guangzhou 510006, PR China
[b] Department of Biology and Chemistry, City University of Hong Kong, 83 Tat Chee Avenue, Kowloon, Hong Kong, PR China

ARTICLE INFO

Article history:
Received 27 February 2014
Received in revised form 25 April 2014
Accepted 5 May 2014
Available online 10 May 2014

Keywords:
Alzheimer's disease
Imidazole derivative
Aβ aggregation
Cholinesterase
Anti-oxidation

ABSTRACT

Background: Alzheimer's disease (AD) is a progressive neurodegenerative brain disorder that is characterized by dementia, cognitive impairment, and memory loss. Diverse factors are related to the development of AD, such as increased level of β-amyloid (Aβ), acetylcholine, metal ion deregulation, hyperphosphorylated tau protein, and oxidative stress.
Methods: The following methods were used: organic syntheses of 1*H*-phenanthro[9,10-*d*]imidazole derivatives, inhibition of self-mediated and metal-induced $A\beta_{1-42}$ aggregation, inhibition studies for acetylcholinesterase and butyrylcholinesterase, anti-oxidation activity studies, CD, MTT assay, transmission electron microscopy, dot plot assay, gel electrophoresis, Western blot, and molecular docking studies.
Results: We synthesized and characterized a new type of 1*H*-phenanthro[9,10-*d*]imidazole derivatives as multifunctional agents for AD treatment. Our results showed that most of these derivatives exhibited strong Aβ aggregation inhibitory activity. Compound **9g** had 74% $A\beta_{1-42}$ aggregation inhibitory effect at 10 μM concentration with its IC_{50} value of 6.5 μM for self-induced $A\beta_{1-42}$ aggregation. This compound also showed good inhibition of metal-mediated (Cu^{2+} and Fe^{2+}) and acetylcholinesterase-induced $A\beta_{1-42}$ aggregation, as indicated by using thioflavin T assay, transmission electron microscopy, gel electrophoresis, and Western blot. Besides, compound **9g** exhibited cholinesterase inhibitory activity, with its IC_{50} values of 0.86 μM and 0.51 μM for acetylcholinesterase and butyrylcholinesterase, respectively. In addition, compound **9g** showed good anti-oxidation effect with oxygen radical absorbance capacity (ORAC) value of 2.29.
Conclusions: Compound **9g** was found to be a potent multi-target-directed agent for Alzheimer's disease.
General significance: Compound **9g** could become a lead compound for further development as a multi-target-directed agent for AD treatment.

1. Introduction

Alzheimer's disease (AD) is the most prevalent form of neurodegeneration which is the most common cause of dementia and other cognitive functions among elderly adults [1–3], with expected number of patients increased to 25 million by 2025 [4]. Over one century since the first description of AD and its predicted increase in incidence in the coming years as well as the lack of effective treatment strategies make this a very important research area [2,5–8]. The molecular etiology of AD remains not completely known, but diverse factors are suggested to be related to the development of AD, including increased level of β-amyloid (Aβ), metal ion deregulation, hyperphosphorylated tau protein, oxidative stress, inflammation, cell cycle regulatory failure, and low level of acetylcholine.

It is well known that Aβ plaques play a central role in the neuropathology of AD [8–12], and the accumulation of aggregated Aβ species in brain tissues has been a key feature of the amyloid cascade hypothesis [10,13–15], which cites that these aggregates are possible causative agents in AD. Therefore, the prevention of Aβ aggregation attracts much current attention. Besides, elevated concentrations of transition

Abbreviations: AAPH, 2,2′-azobis(amidinopropane) dihydrochloride; Aβ, β-amyloid; AChE, acetylcholinesterase; AD, Alzheimer's disease; ATC, acetylthiocholine chloride; BTC, butyrylthiocholine chloride; BuChE, butyrylcholinesterase; CAS, catalytic binding site; ChE, cholinesterase; DCFH-DA, dichlorofluorescein diacetate; DMEM, Dulbecco's modified Eagle's medium; DTNB, 5,5′-dithiobis(2-nitrobenzoic acid); MTDLs, multi-target-directed ligands; MTT, 3-(4,5-dimethyl-2-thiazolyl)-2,5-diphenyl-2H-tetrazolium bromide; ORAC, oxygen radical absorbance capacity; PAS, peripheral anionic site; RMSD, root mean square deviation; ROS, reactive oxygen species; TEM, transmission electron microscopy; ThT, thioflavin T; TLC, thin layer chromatography

* Corresponding author. Tel.: +86 20 3994 3056.
** Corresponding author. Tel.: +86 20 3994 3058.
E-mail addresses: ceshzs@mail.sysu.edu.cn (Z.-S. Huang), liding@mail.sysu.edu.cn (D. Li).

http://dx.doi.org/10.1016/j.bbagen.2014.05.005
0304-4165/

metals such as Fe, Cu, and Zn play important roles in Aβ aggregate deposition [11,16–19] and neurotoxicity as well as inducing formation of reactive oxygen species (ROS) [20–23]. Thus, lowering the concentration of metals in brain by chelating metals represents another rational therapeutic approach for halting AD pathogenesis. In addition, cholinergic hypothesis play important role in the development of AD, acetylcholine can be degraded by two types of cholinesterases, namely acetylcholinesterase (AChE) and butyrylcholinesterase (BuChE) [24]. AChE contains two binding sites: the catalytic active site (CAS) at the bottom and the peripheral anionic site (PAS) near the entrance of the gorge [25]. It has been indicated that AChE promotes amyloid fibril formation by interacting with the PAS of the enzyme, giving stable AChE–Aβ complexes, which are more toxic than single Aβ peptides [26]. Thus, small molecules that could bind the CAS site and the PAS site appear to be very promising therapeutic lead compounds. Due to the multiple factors and the lack of effective drugs, scientists pay more and more attention to the multi-target-directed ligands (MTDLs) designing strategies for AD treatment [27–30].

The benzazole scanffold [31] and benzimidazole derivatives [32,33] have been used in bioactive molecular design for the treatment of AD. Based on these structures, we tried to expand their aromatic plane to improve their π–π interactions and hydrophobic interactions with the targets. The "click" chemistry has been used in the design of AD modulating agents [34]. Here, we report our design, synthesis, and evaluation of 1H-phenanthro[9,10-d]imidazole derivatives as multifunctional inhibitors for the treatment of AD. We found that our compound **9g** showed 74% $A\beta_{1-42}$ aggregation inhibitory effect when used at 10 μM concentration, which is better than resveratrol with only 53% $A\beta_{1-42}$ aggregation inhibitory effect. Compound **9g** could also inhibit and disaggregate metal-induced aggregation of $A\beta_{1-42}$, which was supported by using thioflavin T (ThT) assay, transmission electron microscopy (TEM), and gel electrophoresis. Besides, compound **9g** was found to be potent inhibitor for both AChE and BuChE, with its IC_{50} values of 0.86 μM and 0.51 μM for AChE and BuChE, respectively. In addition, compound **9g** was also found to be an anti-oxidation agent with its oxygen radical absorbance capacity (ORAC) value of 2.29. Thus, compound **9g** could become a lead compound for further development as a multi-target-directed agent for the treatment of AD.

2. Materials and methods

2.1. Materials

All the reagents used in the biological assay were analytically pure. Chemical reagents used in the synthesis were of research grade or better and were obtained from commercial sources.

2.2. Organic syntheses of imidazole derivatives

All the chemical reagents used in the synthesis were of research grade or better and were obtained from commercial sources. ^1H and ^{13}C NMR spectra were recorded using TMS as the internal standard in DMSO-d_6 or $CDCl_3$ with a Bruker BioSpin GmbH spectrometer at 400 MHz and 100 MHz, respectively. High resolution mass spectra (HRMS) were recorded on Shimadzu LCMS-IT-TOF spectrometer. Flash column chromatography was performed with silica gel (200–300 mesh) purchased from Qingdao Haiyang Chemical Co. Ltd. The purities of synthesized compounds were confirmed to be higher than 95% by using analytical HPLC with a dual pump Shimadzu LC-20AB system equipped with an Ultimate-QB-C18 column (4.6 × 250 mm, 5 μm) and eluted with methanol/water (60:40 to 70:30) containing 0.1% trifluoroacetic acid at a flow rate of 0.6 mL/min. Organic syntheses of imidazole derivatives were shown in Schemes 1–4.

2.2.1. General procedure for the preparation of 4-(2-bromoethoxy) benzaldehyde (1), 4-(3-bromopropoxy)benzaldehyde (2), and 4-(4-bromobutoxy)benzaldehyde (3)

To a solution of 4-hydroxybenzaldehyde (20 mmol, 2.44 g) and anhydrous K_2CO_3 (30 mmol, 5.14 g) in 100 mL dry acetone was added 1,2-dibromoethane (40 mmol, 7.51 g) or 1,3-dibromopropane (40 mmol, 8.08 g) or 1,4-dibromobutane (40 mmol, 8.64 g). The resulting mixture was heated under reflux for 6 h until the starting material disappeared, and then the remaining solution was filtered and washed with acetone for three times. After concentration, the crude product was purified with gel chromatography to give desired product **1** or **2** or **3** as a white liquid.

2.2.2. General procedure for the preparation of 2-(4-(bromomethoxy) phenyl)-1H-phenanthro[9,10-d]imidazole (4), 2-(4-(3-bromopropoxy) phenyl)-1H-phenanthro[9,10-d]imidazole (5), and 2-(4-(4-bromobutoxy) phenyl)-1H-phenanthro[9,10-d]imidazole (6)

A mixture of phenanthrene-9,10-dione (10 mmol, 2.08 g) and **1** (11 mmol, 2.51 g) or **2** (11 mmol, 2.66 g) or **3** (11 mmol, 2.82 g) in 50 mL acetic acid was added ammonium acetate (100 mmol, 7.8 g), and the solution was heated under reflux at 120 °C for 2 h, resulting in a gray precipitate. After cooling, the mixture was poured into 100 mL of water and neutralized with concentrated aqueous ammonia. The gray product was filtered and washed with water to give a crude product, which was purified with flash gel chromatography to give compound **4** or **5** or **6** as an off white solid.

2.2.2.1. 2-(4-(bromomethoxy)phenyl)-1H-phenanthro[9,10-d]imidazole (4). The compound was obtained with a yield of 56%. ^1H NMR (400 MHz, DMSO) δ 13.32 (s, 1H), 8.84 (d, J = 8.2 Hz, 2H), 8.55 (d, J = 7.6 Hz, 2H), 8.26 (d, J = 8.4 Hz, 2H), 7.72 (t, J = 7.2 Hz, 2H), 7.62 (t, J = 7.4 Hz, 2H), 7.19 (d, J = 8.4 Hz, 2H), 4.43 (t, J = 5.8 Hz, 2H), 3.86 (t, J = 6.0 Hz, 2H); ^{13}C NMR (100 MHz, DMSO) δ 171.9, 158.8, 149.1, 127.7, 127.5, 127.0, 125.0, 123.8, 123.4, 121.8, 115.0, 67.9, 31.3.

2.2.2.2. 2-(4-(3-bromopropoxy)phenyl)-1H-phenanthro[9,10-d]imidazole (5). The compound was obtained with a yield of 66%. ^1H NMR (400 MHz, $CDCl_3$) δ 8.72 (d, J = 8.4 Hz, 2H), 8.43 (d, J = 8.0 Hz, 2H), 8.01 (d, J = 8.8 Hz,2H), 7.65–7.58 (m, 2H), 6.89 (d, J = 8.4 Hz, 2H), 4.06 (t, J = 5.6 Hz, 2H), 3.72 (t, J = 6.2 Hz, 2H), 2.23–2.17 (m, 2H); ^{13}C NMR (100 MHz, $CDCl_3$) δ 159.2, 149.0, 127.7, 127.3, 127.0, 125.0, 123.7, 123.2, 121.8, 114.8, 67.2, 32.6, 29.8.

2.2.2.3. 2-(4-(4-bromobutoxy)phenyl)-1H-phenanthro[9,10-d]imidazole (6). The compound was obtained with a yield of 58%. ^1H NMR (400 MHz, DMSO) δ 13.31 (s, 1H), 8.85 (d, J = 8.4 Hz, 2H), 8.54 (d, J = 8.0 Hz, 2H), 8.24 (d, J = 8.8 Hz, 2H), 7.72 (t, J = 7.4 Hz, 2H), 7.63 (t, J = 7.4 Hz, 2H), 7.16 (d, J = 8.8 Hz, 2H), 4.12 (t, J = 6.2 Hz, 2H), 3.64 (t, J = 6.6 Hz, 2H), 2.05–1.95 (m, 2H), 1.89–1.82 (m, 2H); ^{13}C NMR (100 MHz, DMSO) δ 159.5, 149.2, 127.7, 127.4, 127.0, 125.0, 123.8, 122.9, 121.8, 114.8, 66.8, 34.7, 29.1, 27.4.

2.2.3. General procedure for the preparation of 7a–9f

To a stirred suspension of compound **4** or **5** or **6** (1 mmol) and anhydrous K_2CO_3 (2 mmol) in dry acetonitrile (50 mL) was added excess alkylamine (3 mmol), and the resulting mixture was heated under reflux for 6 h until the starting material disappeared. The K_2CO_3 was removed through filtration, and the remaining solution was concentrated under reduced pressure. The crude product was purified by using gel chromatography with CH_2Cl_2/MeOH (30:1 to 10:1) as elution solvents to give the desired products.

2.2.3.1. 2-(4-(1H-phenanthro[9,10-d]imidazol-2-yl)phenoxy)-N,N-diethylethanamine (7a). Compound **4** was treated with diethylamine following the general procedure to give the desired product **7a** as a

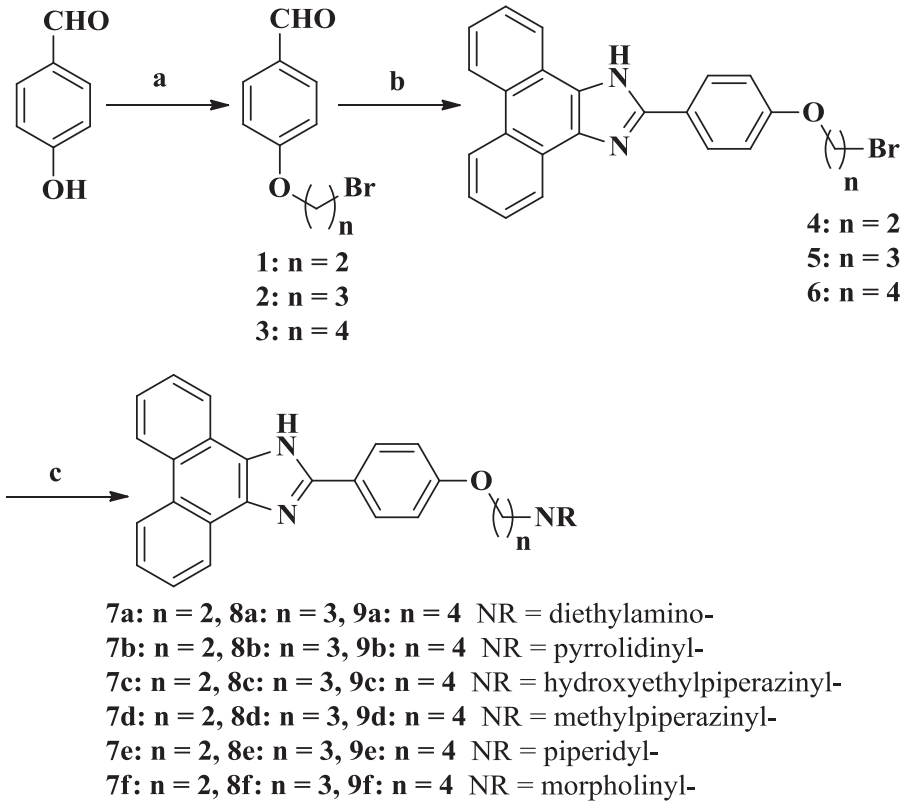

Scheme 1. The organic synthesis of target compounds **7a–9f**. Reagents and conditions: (a) 1,2-dibromoethane or 1,3-dibromopropane, or 1,4-dibromobutane, K_2CO_3, acetone, reflux 6 h; (b) phenanthrene-9,10-dione, NH_4OAc, AcOH, 120 °C, 3 h; (c) RNH, K_2CO_3, acetonitrile, reflux, 5–6 h.

white solid with a yield of 62%, with purity of 98% determined by using HPLC. ^{1}H NMR (400 MHz, DMSO) δ 13.30 (s, 1H), 8.87 (d, J = 8.4 Hz, 1H), 8.84 (d, J = 8.4 Hz, 1H), 8.58 (d, J = 7.8 Hz, 1H), 8.58 (d, J = 8.0 Hz, 1H), 7.77–7.70 (m, 2H), 7.65–7.58 (m, 2H), 4.17 (t, J = 5.6 Hz, 2H), 2.92 (t, J = 5.6 Hz, 2H), 2.76–2.57 (m, 4H), 1.04 (t, J = 7.0 Hz, 6H); ^{13}C NMR (100 MHz, DMSO) δ 159.3, 149.3, 136.9, 127.7, 127.4, 127.0, 125.0, 124.9 124.0, 123.6, 123.1, 122.4, 121.9, 114.8, 66.0, 51.1, 47.0, 11.4. ESI-HRMS m/z: calcd for $C_{27}H_{27}N_3O$ $[M + H]^+$ 410.2227, found 410.2245.

2.2.3.2. 2-(4-(2-(pyrrolidin-1-yl)ethoxy)phenyl)-1H-phenanthro[9,10-d]imidazole (7b). Compound **4** was treated with pyrrolidine following the general procedure to give the desired product **7b** as a light grey solid with a yield of 47%, with purity of 98% determined by using HPLC. ^{1}H NMR (400 MHz, DMSO) δ 13.37 (s, 1H), 8.88–8.83 (m, 2H), 8.59 (d, J = 7.2 Hz, 2H), 8.30–8.28 (m, 2H), 7.76 (d, J = 7.2 Hz, 1H), 7.72 (d, J = 9.0 Hz, 1H), 7.63 (t, J = 7.4 Hz, 2H), 7.20–7.18 (m, 2H), 4.23 (t, J = 5.2 Hz, 2H), 3.01 (t, J = 5.2 Hz, 2H), 3.81–2.68 (m, 4H), 1.82–1.73 (m, 4H); ^{13}C NMR (100 MHz, DMSO) δ 159.2, 149.2, 136.8, 127.7, 127.4, 127.0, 125.0, 124.0 123.7, 123.2, 122.4, 121.9, 114.8, 66.2, 54.0, 23.0. ESI-HRMS m/z: calcd for $C_{27}H_{25}N_3O$ $[M + H]^+$ 408.2070, found 408.2072.

2.2.3.3. 2-(4-(2-(4-(1H-phenanthro[9,10-d]imidazol-2-yl)phenoxy)ethyl)piperazin-1-yl)ethanol (7c). Compound **4** was treated with *N*-(2-hydroxyethyl)piperazine following the general procedure to give the desired product **7c** as a white solid with a yield of 28%, with purity of 95% determined by using HPLC. ^{1}H NMR (400 MHz, MeOD) δ 8.66 (d, J = 8.4 Hz, 2H), 8.41 (d, J = 7.6 Hz, 2H), 8.03 (d, J = 8.8 Hz, 2H), 7.57 (t, J = 7.2 Hz, 2H), 7.50 (t, J = 7.0 Hz, 2H), 6.98 (d, J = 8.8 Hz, 2H), 4.07 (t, J = 5.2 Hz, 2H), 3.69 (t, J = 5.4 Hz, 2H), 3.02–2.90 (m, 4H), 2.89–2.80 (m, 4H), 2.80–2.68 (m, 4H); ^{13}C NMR (100 MHz, MeOD) δ 161.1, 151.4, 129.6, 129.3, 128.1 126.4, 125.9 124.8, 124.2, 123.0, 116.0, 66.4, 60.1, 57.8, 57.4 53.3, 52.3. ESI-HRMS m/z: calcd for $C_{29}H_{30}N_4O_2$ $[M + H]^+$ 467.2442, found 467.2451.

2.2.3.4. 2-(4-(2-(4-methylpiperazin-1-yl)ethoxy)phenyl)-1H-phenanthro[9,10-d]imidazole (7d). Compound **4** was treated with *N*-methyl piperazine following the general procedure to give the desired product **7d** as a white solid with a yield of 45%, with purity of 95% determined by using

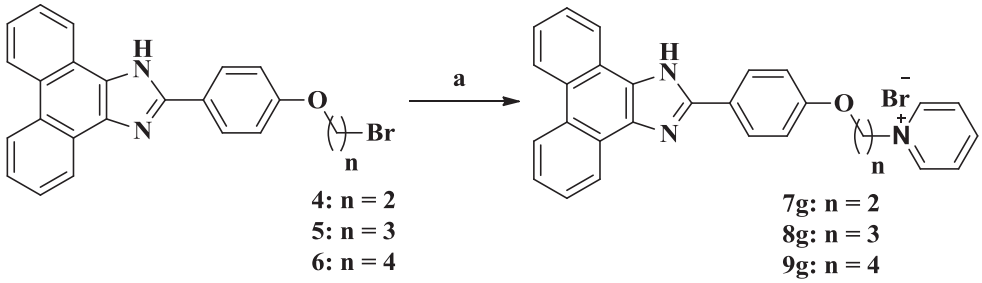

Scheme 2. The organic synthesis of target compounds **7g–9g**. Reagents and conditions: (a) pyridine, 80 °C, 8 h.

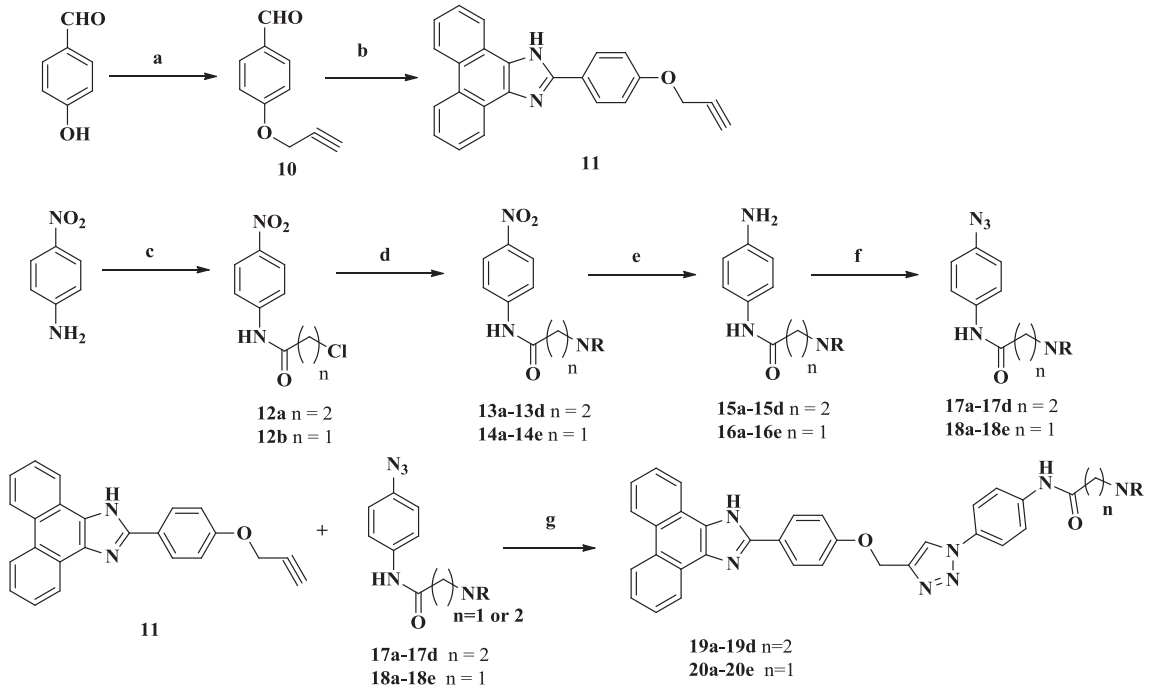

Scheme 3. The organic synthesis of target compounds **19a–20e**. Reagents and conditions: (a) propargyl bromide, K_2CO_3, acetone, reflux 6 h; (b) phenanthrene-9,10-dione, NH_4OAc, AcOH, 120 °C, 3 h; (c) chloroacetyl chloride or 3-chloropropionyl chloride, THF, K_2CO_3, 0 °C to 50 °C, 16 h; (d) CH_3OH, THF, 0 °C to rt, 16 h; (e) NH_4CO_2, Pb/C, DMF, rt, 4 h; (f) conc. HCl, *t*-BuONO, NaN_3, H_2O; (g) sodium ascorbate, $CuSO_4{\cdot}5H_2O$, *t*-BuOH, H_2O.

HPLC. ^{1}H NMR (400 MHz, DMSO) δ 13.28 (s, 1H), 8.88 (d, J = 8.4 Hz, 1H), 8.84 (d, J = 8.4 Hz, 1H), 8.58 (d, J = 8.0 Hz, 1H), 8.54 (d, J = 8.0 Hz, 1H), 8.25 (d, J = 8.8 Hz, 2H), 7.76–7.70 (m, 2H), 7.63 (t, J = 6.4 Hz, 2H), 7.17 (d, J = 8.8 Hz, 2H), 4.18 (t, J = 5.8 Hz, 2H), 2.74 (t, J = 5.8 Hz, 2H), 2.52–2.49 (m, 4H), 2.43–2.38 (m, 4H), 2.19 (s, 3H); ^{13}C NMR (100 MHz, DMSO) δ 159.4, 149.3, 127.6, 127.4, 127.0, 125.0, 124.0, 123.6, 123.0, 121.8, 114.8, 65.7, 56.5, 54.6, 52.8, 45.5. ESI-HRMS m/z: calcd for $C_{28}H_{28}N_4O$ $[M + H]^+$ 437.2336, found 437.2352.

2.2.3.5. 2-(4-(2-(piperidin-1-yl)ethoxy)phenyl)-1H-phenanthro[9,10-d] imidazole (7e). Compound **4** was treated with piperidine following the general procedure to give the desired product **7e** as a white solid with a yield of 73%, with purity of 99% determined by using HPLC. ^{1}H NMR

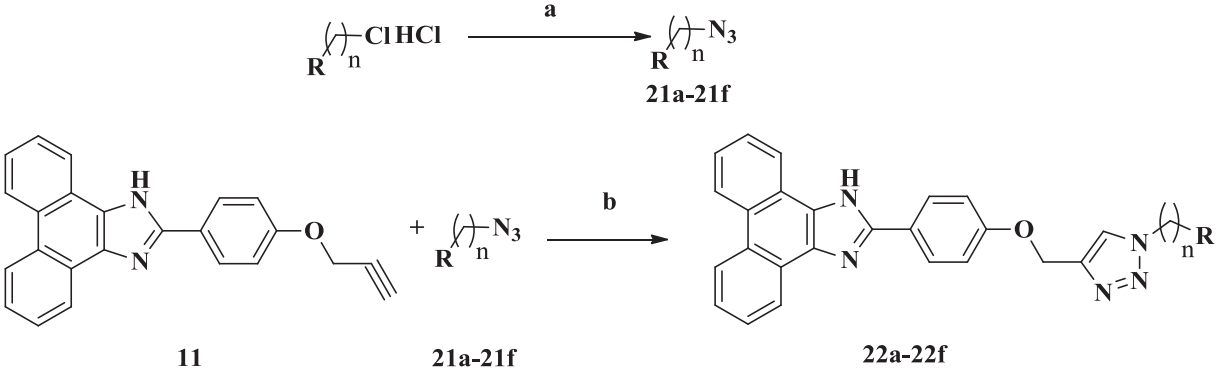

Scheme 4. The organic synthesis of target compounds **22a–22f**. Reagents and conditions: (a) NaN_3, H_2O; (b) sodium ascorbate, $CuSO_4{\cdot}5H_2O$, *t*-BuOH, H_2O.

(400 MHz, DMSO) δ 13.34 (s, 1H), 8.84 (t, J = 9.4, 2H), 8.63 (d, J = 7.2 Hz, 1H), 8.58 (d, J = 7.6 Hz, 1H), 8.29 (d, J = 8.0 Hz, 2H), 7.75 (d, J = 6.8 Hz, 2H), 7.63 (t, J = 6.8 Hz, 2H), 7.18 (d, J = 8.4 Hz, 2H), 4.16 (t, J = 5.8 Hz, 2H), 2.73 (t, J = 5.4 Hz, 2H), 2.53–2.42 (m, 4H), 1.57–1.46 (m, 4H), 1.42–1.33 (m, 2H); ^{13}C NMR (100 MHz, DMSO) δ 159.4, 149.3, 136.9, 127.7, 127.4, 127.0, 125.0, 124.9, 124.0, 123.6, 123., 122.4, 121.8, 114.8, 65.5, 57.2, 54.3, 25.4, 23.7. ESI-HRMS m/z: calcd for $C_{28}H_{28}N_3O$ $[M + H]^+$ 422.2227, found 422.2228.

2.2.3.6. 4-(2-(4-(1H-phenanthro[9,10-d]imidazol-2-yl)phenoxy)ethyl) morpholine (7f). Compound **4** was treated with morpholine following the general procedure to give the desired product **7f** as an off white solid with a yield of 65%, with purity of 99% determined by using HPLC. ^{1}H NMR (400 MHz, DMSO) δ 13.29 (s, 1H), 8.88–8.83 (m, 2H), 8.58 (d, J = 8.0 Hz, 1H), 8.54 (d, J = 8.0 Hz, 1H), 8.28 (d, J = 2.8 Hz, 1H), 8.28 (d, J = 2.4 Hz, 1H), 7.77–7.70 (m, 2H), 7.63 (t, J = 6.8 Hz, 2H), 7.19 (d, J = 2.4 Hz, 2H), 7.17 (d, J = 2.0 Hz, 2H), 4.20 (t, J = 6.0 Hz, 2H), 3.66–3.56 (m, 4H), 2.75 (t, J = 5.8 Hz, 2H), 2.53–2.49 (m, 4H); ^{13}C NMR (100 MHz, DMSO) δ 159.4, 149.2, 127.7, 127.4, 127.0, 125.0, 124.0, 123.7, 123.0, 121.8, 114.9, 66.1, 65.5, 57.0, 53.6. ESI-HRMS m/z: calcd for $C_{27}H_{25}N_3O_2$ $[M + H]^+$ 424.2020, found 424.2035.

2.2.3.7. 3-(4-(1H-phenanthro[9,10-d]imidazol-2-yl)phenoxy)-N,N-diethylpropan-1-amine (8a). Compound **5** was treated with diethylamine following the general procedure to give the desired product **8a** as a white solid with a yield of 38%, with purity of 99% determined by using HPLC. ^{1}H NMR (400 MHz, DMSO) δ 9.07 (s, 1H), 8.87 (d, J = 7.6 Hz, 2H), 8.57 (d, J = 7.6 Hz, 2H), 8.29 (d, J = 6.4 Hz, 2H), 7.75 (t, J = 7.0 Hz, 2H), 7.65 (t, J = 7.0 Hz, 2H), 7.21 (d, J = 6.4 Hz, 2H), 4.21 (t, J = 5.8 Hz, 2H), 3.35 (t, J = 5.6 Hz, 2H), 3.23–3.18 (m, 4H), 2.22–2.09 (m, 2H), 1.24 (t, J = 7.0 Hz, 6H); ^{13}C NMR (100 MHz, DMSO) δ 159.2, 149.0, 127.9, 127.5, 127.1, 125.2, 123.9, 122.8, 121.8, 114.9, 64.9, 48.1, 46.6, 23.3, 8.6. ESI-HRMS m/z: calcd for $C_{28}H_{29}N_3O$ $[M + H]^+$ 424.2383, found 424.2396.

2.2.3.8. 2-(4-(3-(pyrrolidin-1-yl)propoxy)phenyl)-1H-phenanthro[9,10-d]imidazole (8b). Compound **5** was treated with pyrrolidine following the general procedure to give the desired product **8b** as a light grey solid with a yield of 32%, with purity of 99% determined by using HPLC. ^{1}H NMR (400 MHz, DMSO) δ 13.35 (s, 1H), 8.87 (d, J = 8.4 Hz, 1H), 8.84 (d, J = 8.4 Hz, 1H), 8.58 (d, J = 7.6 Hz, 2H), 8.28 (d, J = 8.4 Hz, 2H), 7.75 (d, J = 7.6 Hz, 1H), 7.71 (d, J = 7.6 Hz, 1H), 7.63 (t, J = 6.0 Hz, 2H), 7.17 (d, J = 8.8 Hz, 2H), 4.16 (t, J = 5.8 Hz, 2H), 3.01–2.91 (m, 4H), 2.11–2.03 (m, 2H), 1.90–1.78 (m, 4H); ^{13}C NMR (100 MHz, DMSO) δ 159.3, 149.2, 136.8, 127.7, 127.4, 127.0, 125.0, 124.9, 124.0, 1237, 123.1, 122.4, 122.0, 121.8, 99.5, 65.4, 53.3, 51.7, 26.5, 22.8. ESI-HRMS m/z: calcd for $C_{28}H_{27}N_3O$ $[M + H]^+$ 422.2227, found 422.2227.

2.2.3.9. 2-(4-(3-(4-(1H-phenanthro[9,10-d]imidazol-2-yl)phenoxy) propyl)piperazin-1-yl)ethanol (8c). Compound **5** was treated with *N*-(2-hydroxyethyl)piperazine following the general procedure to give the desired product **8c** as a white solid with a yield of 59%, with purity of 99% determined by using HPLC. ^{1}H NMR (400 MHz, MeOD) δ 8.64 (d, J = 8.4 Hz, 2H), 8.40 (d, J = 7.6 Hz, 2H), 7.99 (d, J = 8.4 Hz, 2H), 7.56 (t, J = 7.4 Hz, 2H), 7.49 (t, J = 7.2 Hz, 2H), 6.90 (d, J = 8.8 Hz, 2H), 3.87 (t, J = 5.8 Hz, 2H), 3.59 (t, J = 5.8 Hz, 2H), 2.59–2.46 (m, 12H), 1.85–1.79 (m, 2H); ^{13}C NMR (100 MHz, MeOD) δ 161.6, 151.6, 129.6, 129.3, 128.1, 126.4, 124.8, 124.0, 122.9, 115.9, 67.1, 60.8, 59.2, 55.9, 53.7, 53.2, 27.2. ESI-HRMS m/z: calcd for $C_{30}H_{32}N_4O_2$ $[M + H]^+$ 481.2598, found 481.2597.

2.2.3.10. 2-(4-(3-(4-methylpiperazin-1-yl)propoxy)phenyl)-1H-phenanthro[9,10-d]imidazole (8d). Compound **5** was treated with *N*-methyl piperazine following the general procedure to give the desired product **8d** as a white solid with a yield of 41%, with purity of 99% determined by using HPLC. ^{1}H NMR (400 MHz, DMSO) δ 13.30 (s, 1H), 8.85 (s, 2H), 8.59–8.54 (m, 2H), 8.25 (d, J = 6.8 Hz, 2H), 7.73 (d, J = 6.4 Hz, 2H), 7.63 (t, J = 7.2 Hz, 2H), 7.15 (d, J = 6.8 Hz, 2H), 4.10 (t, J = 5.4 Hz, 2H), 2.45 (t, J = 6.2 Hz, 2H), 2.39–2.34 (m, 8H), 2.16 (s, 3H), 1.94–1.89 (m, 2H); ^{13}C NMR (100 MHz, DMSO) δ 159.5, 149.3, 127.7, 127.4, 127.0, 125.0, 123.9, 122.9, 121.8, 114.8, 66.0, 54.7, 54.3, 52.7, 45.7, 26.2. ESI-HRMS m/z: calcd for $C_{29}H_{30}N_4O$ $[M + H]^+$ 451.2492, found 451.2503.

2.2.3.11. 2-(4-(3-(piperidin-1-yl)propoxy)phenyl)-1H-phenanthro[9,10-d]imidazole (8e). Compound **5** was treated with piperidine following the general procedure to give the desired product **8e** as a white solid with a yield of 33%, with purity of 99% determined by using HPLC. ^{1}H NMR (400 MHz, DMSO) δ 13.31 (s, 1H), 8.85 (d, J = 8.0 Hz, 2H), 8.56 (d, J = 7.6 Hz, 2H), 8.25 (d, J = 8.8 Hz, 2H), 7.73 (t, J = 7.4 Hz, 2H), 7.65–7.61 (m, 2H), 7.15 (d, J = 8.8 Hz, 2H), 4.10 (t, J = 6.4 Hz, 2H), 2.46 (t, J = 7.2 Hz, 2H), 2.42–2.35 (m, 4H), 1.91 (s, 2H), 1.56–1.48 (m, 4H), 1.43–1.36 (m, 2H); ^{13}C NMR (100 MHz, DMSO) δ 172.3, 159.5, 149.3, 127.7, 127.4, 126.9, 124.9, 123.8, 123.0, 121.9, 114.7, 66.0, 54.9, 53.8, 25.9, 25.2, 23.8, 21.3. ESI-HRMS m/z: calcd for $C_{29}H_{30}N_3O$ $[M + H]^+$ 436.2383, found 436.2384.

2.2.3.12. 4-(3-(4-(1H-phenanthro[9,10-d]imidazol-2-yl)phenoxy)propyl) morpholine (8f). Compound **5** was treated with morpholine following the general procedure to give the desired product **8f** as an off white solid with a yield of 52%, with purity of 99% determined by using HPLC. ^{1}H NMR (400 MHz, DMSO) δ 13.28 (s, 1H), 8.87 (d, J = 8.4 Hz, 1H), 8.84 (d, J = 8.4 Hz, 1H), 8.58 (d, J = 7.6 Hz, 1H), 8.54 (d, J = 7.6 Hz, 2H), 8.25 (d, J = 8.4 Hz, 2H), 7.77–7.70 (m, 2H), 7.63 (m, 2H), 7.16 (d, J = 8.4 Hz, 2H), 4.12 (t, J = 6.4 Hz, 2H), 3.59 (t, J = 4.4 Hz, 2H), 2.46 (t, J = 7.0 Hz, 2H), 2.42–2.33 (m, 2H), 1.96–1.89 (m, 2H); ^{13}C NMR (100 MHz, DMSO) δ 159.5, 149.3, 136.9, 127.7, 127.4, 127.3, 127.0, 125.0, 124.9, 124.0, 123.7, 122.9, 122.4, 121.8, 114.8, 66.1, 66.0, 54.8, 53.3, 25.8. ESI-HRMS m/z: calcd for $C_{28}H_{27}N_3O_2$ $[M + H]^+$ 438.2176, found 438.2192.

2.2.3.13. 4-(4-(1H-phenanthro[9,10-d]imidazol-2-yl)phenoxy)-N,N-diethylbutan-1-amine (9a). Compound **6** was treated with diethylamine following the general procedure to give the desired product **9a** as a white solid with a yield of 45%, with purity of 99% determined by using HPLC. ^{1}H NMR (400 MHz, DMSO) δ 13.38 (s, 1H), 8.92–8.87 (m, 2H), 8.62 (d, J = 6.8 Hz, 2H), 8.31 (d, J = 7.6 Hz, 2H), 7.81–7.75 (m, 2H), 7.69–7.66 (m, 2H), 7.20 (d, J = 8.0 Hz, 2H), 4.15 (t, J = 6.0 Hz, 2H), 2.67 (m, 6H), 1.86–1.80 (m, 2H), 1.71–1.64 (m, 2H), 1.07 (t, J = 6.8 Hz, 6H); ^{13}C NMR (100 MHz, DMSO) δ 159.4, 149.3, 136.8, 129.3, 127.8, 127.4, 127.0, 125.0, 123.9, 123.7, 123.1, 122.5, 122.1, 121.9, 118.7, 115.2, 114.8, 67.0, 53.8, 53.1, 25.9, 22.6, 22.5. ESI-HRMS m/z: calcd for $C_{29}H_{31}ON_3$ $[M + H]^+$ 438.2540, found 438.2543.

2.2.3.14. 2-(4-(4-(pyrrolidin-1-yl)butoxy)phenyl)-1H-phenanthro[9,10-d]imidazole (9b). Compound **6** was treated with pyrrolidine following the general procedure to give the desired product **9b** as a light grey solid with a yield of 38%, with purity of 99% determined by using HPLC. ^{1}H NMR (400 MHz, DMSO) δ 13.38 (s, 1H), 8.92–8.87 (m, 2H), 8.62 (d, J = 6.4 Hz, 2H), 8.31 (d, J = 7.6 Hz, 2H), 7.81–7.74 (m, 2H), 7.71–7.63 (m, 2H), 7.20 (d, J = 8.0 Hz, 2H), 4.15 (t, J = 6.0 Hz, 2H), 2.72–2.60 (m, 6H), 1.85–1.80 (m, 2H), 1.71–1.64 (m, 2H), 1.07 (t, J = 6.8 Hz, 6H); ^{13}C NMR (100 MHz, DMSO) δ 159.5, 149.3, 136.8, 127.7, 127.4, 126.9, 124.9, 123.9, 123.7, 122.9, 121.9, 114.8, 67.5, 51.5, 46.2, 26.4, 22.4, 10.9. ESI-HRMS m/z: calcd for $C_{29}H_{30}ON_3$ $[M + H]^+$ 436.2383, found 436.2385.

2.2.3.15. 2-(4-(4-(4-(1H-phenanthro[9,10-d]imidazol-2-yl)phenoxy) butyl)piperazin-1-yl)ethanol (9c). Compound **6** was treated with *N*-(2-hydroxyethyl)piperazine following the general procedure to give the desired product **9c** as a white solid with a yield of 75%,

with purity of 99% determined by using HPLC. ^{1}H NMR (400 MHz, DMSO) δ 13.34 (s, 1H), 8.87–8.82 (m, 2H), 8.59 (d, J = 6.8 Hz, 2H), 8.27 (d, J = 8.0 Hz, 2H), 7.74–7.70 (m, 2H), 7.63 (d, J = 6.8 Hz, 2H), 7.15 (d, J = 8.0 Hz, 2H), 4.59 (s, 1H), 4.10 (t, J = 5.4 Hz, 2H), 3.55 (t, J = 5.8 Hz, 2H), 3.36 (t, J = 5.8 Hz, 2H), 2.78–2.54 (m, 10H), 1.86–1.73 (m, 2H), 1.72–1.55 (m, 2H); ^{13}C NMR (100 MHz, DMSO) δ 159.5, 149.3, 136.8, 127.8, 127.4, 126.9, 125.0, 124.0, 123.6, 122.9, 122.5, 122.1, 121.8, 114.8, 67.4, 59.5, 57.7, 56.8, 52.2, 51.6, 26.4, 22.2. ESI-HRMS m/z: calcd for $C_{31}H_{35}O_2N_4$[M + H]$^+$ 495.2755, found 495.2759.

2.2.3.16. 2-(4-(4-(4-methylpiperazin-1-yl)butoxy)phenyl)-1H-phenanthro[9,10-d]imidazole (9d). Compound **6** was treated with *N*-methyl piperazine following the general procedure to give the desired product **9d** as a white solid with a yield of 37%, with purity of 99% determined by using HPLC. ^{1}H NMR (400 MHz, DMSO) δ 13.30 (s, 1H), 8.45 (t, J = 10.0, 2H), 8.58 (t, J = 8.2 Hz, 2H), 8.26 (d, J = 8.4 Hz, 2H), 7.75 (d, J = 7.6 Hz, 1H), 7.71 (d, J = 7.6 Hz, 1H), 7.62 (t, J = 7.0 Hz, 2H), 7.15 (d, J = 8.4 Hz, 2H), 4.08 (t, J = 6.2 Hz, 2H), 2.50 (t, J = 5.8 Hz, 2H), 2.48–2.36 (m, 8H), 2.25 (s, 3H), 1.81–1.73 (m, 2H), 1.64–1.56 (m, 2H); ^{13}C NMR (100 MHz, DMSO) δ 159.5, 149.3, 136.9, 127.7, 127.4, 126.9, 125.0, 124.0, 123.6, 122.9, 122.4, 121.9, 114.7, 67.4, 57.0, 54.2, 52.0, 45.1, 26.5, 22.5. ESI-HRMS m/z: calcd for $C_{30}H_{33}ON_4$[M + H]$^+$ 465.2649, found 465.2653.

2.2.3.17. 2-(4-(4-(piperidin-1-yl)butoxy)phenyl)-1H-phenanthro[9,10-d]imidazole (9e). Compound **6** was treated with piperidine following the general procedure to give the desired product **9e** as a white solid with a yield of 23%, with purity of 99% determined by using HPLC. ^{1}H NMR (400 MHz, DMSO) δ 13.36 (s, 1H), 8.87 (d, J = 8.8 Hz, 1H), 8.84 (d, J = 8.8 Hz, 1H), 8.58 (d, J = 7.6 Hz, 2H), 8.27 (d, J = 8.8 Hz, 2H), 7.75 (d, J = 8.0 Hz, 1H), 7.71 (d, J = 8.0 Hz, 1H), 7.63 (t, J = 6.8 Hz, 2H), 7.15 (d, J = 8.4 Hz, 2H), 4.09 (t, J = 6.2 Hz, 2H), 3.35 (m, 2H), 2.48–2.33 (m, 4H), 1.80–1.73 (m, 2H), 1.68–1.61 (m, 2H), 1.59–1.50 (m, 4H), 1.44–1.37 (m, 2H); ^{13}C NMR (100 MHz, DMSO) δ 159.5, 149.3, 136.8, 127.7, 127.4, 126.9, 124.9, 123.9, 123.6, 122.9, 122.5, 122.0, 121.8, 114.7, 99.5, 67.4, 57.6, 53.5, 48.6, 26.5, 24.9, 23.6, 22.2. ESI-HRMS m/z: calcd for $C_{30}H_{32}ON_3$ [M + H]$^+$ 450.2540, found 450.2540.

2.2.3.18. 4-(4-(4-(1H-phenanthro[9,10-d]imidazol-2-yl)phenoxy)butyl) morpholine (9f). Compound **6** was treated with morpholine following the general procedure to give the desired product **9f** as an off white solid with a yield of 74%, with purity of 99% determined by using HPLC. ^{1}H NMR (400 MHz, DMSO) δ 13.27 (s, 1H), 8.85 (d, J = 8.4 Hz, 2H), 8.56 (d, J = 7.6 Hz, 2H), 8.25 (d, J = 8.8 Hz, 2H), 7.73 (t, J = 7.4 Hz, 2H), 7.62 (t, J = 7.0 Hz, 2H), 7.15 (d, J = 8.8 Hz, 2H), 4.09 (t, J = 6.4 Hz, 2H), 3.57 (t, J = 4.6 Hz, 4H), 2.37–2.31 (m, 8H), 1.81–1.74 (m, 2H), 1.63–1.56 (m, 2H); ^{13}C NMR (100 MHz, DMSO) δ 159.6, 149.3, 127.7, 127.4, 126.9, 124.9, 123.8, 122.9, 121.8, 114.8, 67.5, 66.2, 57.7, 53.3, 26.5, 22.3. ESI-HRMS m/z: calcd for $C_{29}H_{30}O_2N_3$ [M + H]$^+$ 452.2333, found 452.2336.

2.2.4. General procedure for the preparation of 7g, 8g, and 9g

A solution of **4** or **5** or **6** (0.5 mmol) in pyridine (5 mL) was heated for 8 h at 80 °C. 5 mL of ether was added to cooled reaction mixture and the pale yellow precipitate was collected by filtration. The precipitate was washed with ether three times and dried under vacuum to give **7g**, **8g**, or **9g**.

2.2.4.1. 1-(2-(4-(1H-phenanthro[9,10-d]imidazol-2-yl)phenoxy)ethyl) pyridin-1-ium bromide (7g). Compound **4** was treated with pyridine following the general procedure to give the desired product **7g** as a yellow solid with a yield of 85%, with purity of 96% determined by using HPLC. ^{1}H NMR (400 MHz, DMSO) δ 13.36 (s, 1H), 9.22 (d, J = 6.4 Hz, 2H), 8.86 (s, 2H), 8.69 (t, J = 7.2 Hz, 2H), 8.57 (d, J = 7.6 Hz, 2H), 8.31–8.21 (m, 4H), 7.77–7.70 (m, 2H), 7.63 (t, J = 7.2 Hz, 2H), 7.18 (d, J = 2.0 Hz, 1H), 7.15 (d, J = 2.0 Hz, 1H), 5.13 (t, J = 6.4 Hz, 2H), 4.66 (t, J = 6.4 Hz, 2H); ^{13}C NMR (100 MHz, DMSO) δ 158.3, 149.0, 146.1, 145.5, 127.8, 127.5, 127.0, 1251, 123.9, 121.9, 115.0, 66.2, 59.9. ESI-HRMS m/z: calcd for $C_{28}H_{21}N_3O$ [M–Br + H]$^+$ 416.1757, found 416.1772.

2.2.4.2. 1-(3-(4-(1H-phenanthro[9,10-d]imidazol-2-yl)phenoxy)propyl) pyridin-1-ium bromide (8g). Compound **5** was treated with pyridine following the general procedure to give the desired product **8g** as a yellow solid with a yield of 76%, with purity of 98% determined by using HPLC. ^{1}H NMR (400 MHz, DMSO) δ 13.37 (s, 1H), 9.21 (s, 2H), 8.86 (d, J = 6.4 Hz, 2H), 8.68–8.64 (m, 1H), 8.60 (d, J = 6.4 Hz, 2H), 8.28 (d, J = 7.2 Hz, 2H), 8.23–8.14 (m, 2H), 7.79–7.69 (m, 2H), 7.68–7.57 (m, 2H), 7.02 (d, J = 7.6 Hz, 2H), 4.88 (t, J = 6.4 Hz, 2H), 4.23 (t, J = 6.4 Hz, 2H); ^{13}C NMR (100 MHz, DMSO) δ 158.8, 149.2, 145.6, 145.0, 127.9, 127.4, 127.0, 125.0, 123.8, 123.2, 122.0, 114.7, 65.0, 58.8, 29.9. ESI-HRMS m/z: calcd for $C_{29}H_{23}N_3O$ [M–Br + H]$^+$ 430.1914, found 430.1917.

2.2.4.3. 1-(2-(4-(1H-phenanthro[9,10-d]imidazol-2-yl)phenoxy)ethyl) pyridin-1-ium bromide (9g). Compound **6** was treated with pyridine following the general procedure to give the desired product **9g** as a yellow solid with a yield of 82%, with purity of 99% determined by using HPLC. ^{1}H NMR (400 MHz, DMSO) δ 13.31 (s, 1H), 9.18 (d, J = 5.6 Hz, 2H), 8.85 (s, 2H), 8.66–8.57 (m, 4H), 8.28 (d, J = 8.8 Hz, 2H), 8.20 (t, J = 6.6 Hz, 2H), 7.73 (s, 2H), 7.63 (t, J = 7.2 Hz, 2H),7.38 (t, J = 6.4 Hz, 1H), 7.16 (d, J = 8.4 Hz, 2H), 4.75 (t, J = 7.2 Hz, 2H), 4.14 (t, J = 5.8 Hz, 2H), 2.20–2.10 (m, 2H), 1.88–1.78 (m, 2H); ^{13}C NMR (100 MHz, DMSO) δ 159.8, 150.0, 149.7, 146.0, 145.2, 136.6, 128.6, 128.2, 127.9, 127.5, 125.5, 124.3, 123.6, 122.4, 115.3, 67.4, 60.9, 28.2, 25.7. ESI-HRMS m/z: calcd for $C_{30}H_{26}N_3O$ [M–Br + H]$^+$ 444.2070, found 444.2071.

2.2.5. General procedure for the preparation of 4-(prop-2-yn-1-yloxy) benzaldehyde (10)

To a solution of 4-hydroxybenzaldehyde (10 mmol, 1.22 g) and anhydrous K_2CO_3 (15 mmol, 2.57 g) in 100 mL dry acetone was added propargyl bromide (30 mmol, 3.57 g). The resulting mixture was heated under reflux for 6 h until the starting material disappeared, and then the remaining solution was filtered and washed with acetone for three times. After concentration, the desired product **10** was obtained as a yellow solid with nearly 100% yield.

2.2.6. General procedure for the preparation of 2-(4-(prop-2-yn-1-yloxy) phenyl)-1H-phenanthro[9,10-d]imidazole (11)

The synthesis of **11** was carried out following the procedure for the synthesis of **4**, **5**, and **6**. The desired product **11** was obtained as a gray solid with 53% yield. ^{1}H NMR (400 MHz, DMSO) δ 13.32 (s, 1H), 8.86 (s, 2H), 8.57 (s, 2H), 8.28 (s, 2H), 7.74 (s, 2H), 7.64 (s, 1H), 7.24 (s, 2H), 4.93 (s, 2H), 3.64 (s, 1H); ^{13}C NMR (100 MHz, DMSO) δ 158.0, 149.1, 136.9, 135.4, 129.2, 129.1, 127.6, 127.4, 127.0, 125.0, 123.7, 121.8, 115.2, 79.0, 78.4, 55.6.

2.2.7. General procedures for the preparation of 12a–12b, 13a–13d, 14a–14e, 15a–15d, 16a–16e, 17a–17d, and 18a–18e

The syntheses of **12a**–**12b**, **13a**–**13d**, **14a**–**14e**, **15a**–**15d**, **16a**–**16e**, **17a**–**17d**, and **18a**–**18e** were carried out following procedures reported previously. All these compounds were prepared and identified by using LC-MS.

2.2.8. General procedures for the preparation of 19a–19d, 20a–20e

To a solution of azide (**17a–18e**, 0.4 mmol, 2 equiv.) dissolved in *t*-BuOH (2.5 mL) and distilled water (2.5 mL) was added the intermediate **11** (0.2 mmol, 1 equiv.), sodium ascorbate (19 mg, 0.10 mmol, 0.5 equiv.) and $CuSO_4 \cdot 5H_2O$ (2 mg, 10 μmol, 5 mol%), and the mixture was heated at 140 °C for 5 h. The reaction was cooled and diluted with distilled water. The crude product was isolated by filtration, washed with ice cold distilled water (2 mL), ether (2 × 2 mL), and

was purified with gel chromatography to give desired product **19a–19d, 20a–20e.**

2.2.8.1. N-(4-(4-((4-(1H-phenanthro[9,10-d]imidazol-2-yl)phenoxy) methyl)-1H-1,2,3-triazol-1-yl)phenyl)-3-(pyrrolidin-1-yl)propanamide (19a). It was obtained with purity of 99% determined by using HPLC. ^{1}H NMR (400 MHz, DMSO) δ 13.33 (s, 1H), 10.36 (s, 1H), 8.92 (s, 1H), 8.87 (d, J = 8.4 Hz, 1H), 8.84 (d, J = 8.4 Hz, 1H), 8.59 (d, J = 7.6 Hz, 1H), 8.59 (d, J = 8.0 Hz, 1H), 8.29 (d, J = 8.8 Hz, 2H), 7.87 (d, J = 9.2 Hz, 2H), 7.81 (d, J = 9.2 Hz, 2H), 7.77–7.70 (m, 2H), 7.66–7.61 (m, 2H), 7.33 (d, J = 8.8 Hz, 2H), 5.36 (s, 2H), 3.39–3.26 (m, 2H), 2.78 (t, J = 6.8 Hz, 2H), 2.57–2.54 (m, 2H), 2.52–2.50 (m, 2H), 1.73–1.68 (m, 4H); ^{13}C NMR (100 MHz, DMSO) δ 170.3, 158.9, 149.2, 143.5, 139.6, 136.9, 131.5, 127.7, 127.4, 127.0, 125.1, 125.0, 124.0, 123.7, 123.5, 122.7, 122.4, 121.8, 120.8, 119.7, 115.1, 61.2, 53.4, 51.3, 35.9, 23.1. ESI-HRMS m/z: calcd for $C_{37}H_{33}N_7O_2$ $[M + H]^+$ 608.2768, found 608.2773.

2.2.8.2. N-(4-(4-((4-(1H-phenanthro[9,10-d]imidazol-2-yl)phenoxy) methyl)-1H-1,2,3-triazol-1-yl)phenyl)-3-(diethylamino)propanamide (19b). It was obtained with purity of 99% determined by using HPLC. ^{1}H NMR (400 MHz, DMSO) δ 13.37 (s, 1H), 10.45 (s, 1H), 8.93 (s, 1H), 8.87 (d, J = 8.4 Hz, 1H), 8.84 (d, J = 8.4 Hz, 1H), 8.57 (t, J = 8.4 Hz, 2H), 8.30 (d, J = 8.0 Hz, 2H), 7.87 (d, J = 8.4 Hz, 1H), 7.84 (d, J = 8.4 Hz, 1H), 7.77–7.70 (m, 2H), 7.66–7.61 (m, 2H), 7.32 (d, J = 8.4 Hz, 2H), 5.36 (s, 2H), 2.92 (t, J = 8.4 Hz, 2H), 2.73–2.64 (m, 4H), 2.58 (t, J = 8.4 Hz, 2H), 1.05 (t, J = 5.8 Hz, 6H); ^{13}C NMR (100 MHz, DMSO) δ 170.2, 158.8, 149.2, 143.5, 139.5, 136.8, 131.6, 127.8, 127.4, 127.0, 126.9, 125.1, 124.9, 124.0, 123.7, 123.5, 122.8, 122.4, 121.9, 121.8, 120.8, 119.7, 115.1, 61.2, 47.9, 46.2, 33.3, 11.0. ESI-HRMS m/z: calcd for $C_{37}H_{35}N_7O_2$ $[M + H]^+$ 610.2925, found 610.2942.

2.2.8.3. N-(4-(4-((4-(1H-phenanthro[9,10-d]imidazol-2-yl)phenoxy) methyl)-1H-1,2,3-triazol-1-yl)phenyl)-3-(piperidin-1-yl)propanamide (19c). It was obtained with purity of 99% determined by using HPLC. ^{1}H NMR (400 MHz, $CDCl_3$) δ 11.65 (s, 1H), 8.74 (t, J = 7.4 Hz, 2H), 8.63 (d, J = 7.6 Hz, 1H), 8.34 (d, J = 6.8 Hz, 3H), 8.05 (s, 1H), 7.74–7.68 (m, 8H), 7.21 (d, J = 7.4 Hz, 2H), 5.40 (s, 2H), 2.71 (t, J = 8.4 Hz, 2H), 2.57–2.50 (m, 6H), 1.76–1.69 (m, 4H), 1.65–1.57 (m, 2H); ^{13}C NMR (100 MHz, $CDCl_3$) δ 171.0, 160.5, 144.7, 144.3, 139.7, 135.6, 132.3, 129.2, 129.0 128.9, 127.4, 127.3, 126.3, 126.2, 126.1, 125.3, 123.9, 123.8, 123.4, 123.0, 121.4, 121.2, 121.0, 120.8, 120.2, 115.2, 62.2, 54.2, 53.6, 32.5, 26.3, 24.1. ESI-HRMS m/z: calcd for $C_{38}H_{35}N_6O_3$ $[M + H]^+$ 623.2763, found 623.2768.

2.2.8.4. N-(4-(4-((4-(1H-phenanthro[9,10-d]imidazol-2-yl)phenoxy) methyl)-1H-1,2,3-triazol-1-yl)phenyl)-3-(4-(2-hydroxyethyl)piperazin-1-yl)propanamide (19d). It was obtained with purity of 99% determined by using HPLC. ^{1}H NMR (400 MHz, DMSO) δ 13.33 (s, 1H), 10.36 (s, 1H), 8.91 (s, 2H), 8.87 (d, J = 8.4 Hz, 1H), 8.84 (d, J = 8.4 Hz, 1H), 8.58 (d, J = 7.6 Hz, 1H), 8.54 (d, J = 8.0 Hz, 1H), 8.28 (d, J = 8.4 Hz, 2H), 7.86 (d, J = 8.8 Hz, 2H), 7.80 (d, J = 8.8 Hz, 2H), 7.77–7.70 (m, 2H), 7.66–7.60 (m, 2H), 7.32 (d, J = 8.4 Hz, 2H), 5.36 (s, 2H), 3.51 (s, 1H), 3.49 (t, J = 8.4 Hz, 2H), 2.65 (t, J = 8.4 Hz, 2H), 2.48–2.37 (m, 10H); ^{13}C NMR (100 MHz, DMSO) δ 170.5, 158.9, 149.2, 143.5, 139.6, 136.8, 131.5, 129.6, 129.3, 127.7, 127.5, 127.4, 127.0, 126.9, 125.1, 125.0, 124.0, 123.6, 123.4, 122.7, 122.4, 121.8, 120.8, 119.7, 115.1, 69.7, 61.2, 60.0, 58.3, 53.6, 53.0, 52.2, 34.1. ESI-HRMS m/z: calcd for $C_{40}H_{42}N_8O_3$ $[M + H]^+$ 667.3140, found 667.3140.

2.2.8.5. N-(4-(4-((4-(1H-phenanthro[9,10-d]imidazol-2-yl)phenoxy) methyl)-1H-1,2,3-triazol-1-yl)phenyl)-2-(pyrrolidin-1-yl)acetamide (20a). It was obtained with purity of 96% determined by using HPLC. ^{1}H NMR (400 MHz, DMSO) δ 13.36 (s, 1H), 10.11 (s, 1H), 8.94 (s, 1H), 8.88–8.83 (m, 2H), 8.60–8.55 (m, 2H), 8.30 (d, J = 8.4 Hz, 2H), 7.88 (m, 4H), 7.77–7.70 (m, 2H), 7.67–7.60 (m, 2H), 7.33 (d, J = 8.4 Hz, 2H), 5.37 (s, 2H), 3.41 (s, 2H), 2.78–2.62 (m, 4H), 1.86–1.70 (m, 4H); ^{13}C NMR (100 MHz, DMSO) δ 168.5, 158.9, 149.2, 143.5, 139.0, 136.9, 131.9, 127.8, 127.4, 127.0, 125.0, 124.0, 123.7, 123.6, 122.7, 122.4, 121.9, 120.7, 120.3, 115.1, 61.2, 59.1, 53.7, 23.3. ESI-HRMS m/z: calcd for $C_{36}H_{31}N_7O_2$ $[M + H]^+$ 594.2612, found 594.2625.

2.2.8.6. N-(4-(4-((4-(1H-phenanthro[9,10-d]imidazol-2-yl)phenoxy) methyl)-1H-1,2,3-triazol-1-yl)phenyl)-2-(diethylamino)acetamide (20b). It was obtained with purity of 99% determined by using HPLC. ^{1}H NMR (400 MHz, DMSO) δ 13.31 (s, 1H), 9.90 (s, 2H), 8.94 (s, 1H), 8.87 (d, J = 8.4 Hz, 1H), 8.84 (d, J = 8.4 Hz, 1H), 8.58 (d, J = 7.6 Hz, 1H), 8.53 (d, J = 8.0 Hz, 1H), 8.28 (d, J = 8.4 Hz, 2H), 7.91–7.85 (m, 4H), 7.78–7.70 (m, 2H), 7.66–7.60 (m, 2H), 7.32 (d, J = 8.4 Hz, 2H), 5.37 (s, 2H), 3.20 (s, 2H), 2.65–2.60 (m, 4H), 1.03 (t, J = 7.0 Hz, 4H); ^{13}C NMR (100 MHz, DMSO) δ 171.2, 159.8, 150.1, 144.5, 139.7, 137.8, 132.8, 128.7, 128.4, 128.3, 127.9, 127.9, 126.0, 125.9, 124.9 124.6, 124.4, 123.7, 123.3, 122.8, 121.6, 121.1, 116.1, 62.1, 58.3, 48.7, 12.8. ESI-HRMS m/z: calcd for $C_{36}H_{34}N_7O_2$ $[M + H]^+$ 596.2769, found 596.2773.

2.2.8.7. N-(4-(4-((4-(1H-phenanthro[9,10-d]imidazol-2-yl)phenoxy) methyl)-1H-1,2,3-triazol-1-yl)phenyl)-2-(piperidin-1-yl)acetamide (20c). It was obtained with purity of 99% determined by using HPLC. ^{1}H NMR (400 MHz, DMSO) δ 13.31 (s, 1H), 9.93 (s, 1H), 8.93 (s, 1H), 8.58 (d, J = 7.6 Hz, 1H), 8.53 (d, J = 7.6 Hz, 1H), 8.28 (d, J = 8.4 Hz, 2H), 7.88 (s, 4H), 7.77–7.70 (m, 2H), 7.67–7.58 (m, 2H), 7.32 (d, J = 8.4 Hz, 2H), 5.36 (s, 2H), 3.11 (s, 2H), 2.58 (s, 2H), 2.49–2.43 (m, 2H), 1.61–1.54 (m, 4H), 1.47–1.38 (m, 2H);^{13}C NMR (100 MHz, DMSO) δ 168.9, 158.9, 149.2, 143.6, 138.9, 136.9, 131.8, 127.7, 127.5, 127.4, 127.0, 126.9 125.1, 125.0, 124.0, 123.6, 123.5, 122.7, 122.4, 121.8, 120.7, 120.2, 115.1, 62.6, 61.2, 54.0, 25.3, 23.5. ESI-HRMS m/z: calcd for $C_{37}H_{34}N_7O_2$ $[M + H]^+$ 608.2769, found 608.2773.

2.2.8.8. N-(4-(4-((4-(1H-phenanthro[9,10-d]imidazol-2-yl)phenoxy) methyl)-1H-1,2,3-triazol-1-yl)phenyl)-2-morpholinoacetamide (20d). It was obtained with purity of 98% determined by using HPLC. ^{1}H NMR (400 MHz, DMSO) δ 13.36 (s, 1H), 10.06 (s, 1H), 8.98 (s, 1H), 8.92 (d, J = 8.4 Hz, 1H), 8.88 (d, J = 8.0 Hz, 1H), 8.63 (d, J = 7.6 Hz, 1H), 8.58 (d, J = 7.6 Hz, 1H), 8.32 (d, J = 8.4 Hz, 2H), 7.92 (s, 4H), 7.82–7.75 (m, 2H), 7.68 (d, J = 3.2 Hz, 2H), 7.37 (d, J = 8.4 Hz, 2H), 5.41 (s, 2H), 3.73–3.67 (m, 4H), 3.22 (s, 2H), 2.62–2.56 (m, 4H); ^{13}C NMR (100 MHz, DMSO) δ 168.4, 158.9, 149.2, 143.6, 138.9, 137.5, 131.9, 127.7, 127.4, 127.0, 125.1, 125.0, 121, 123.6, 123.5, 122.7, 122.4, 121.8, 120.7, 120.3, 115.1, 66.0, 62.0, 61.2, 53.1. ESI-HRMS m/z: calcd for $C_{37}H_{32}N_7O_3$ $[M + H]^+$ 610.2561, found 610.2563.

2.2.8.9. N-(4-(4-((4-(1H-phenanthro[9,10-d]imidazol-2-yl)phenoxy) methyl)-1H-1,2,3-triazol-1-yl)phenyl)-2-(dimethylamino)acetamide (20e). It was obtained with purity of 99% determined by using HPLC. ^{1}H NMR (400 MHz, DMSO) δ 13.31 (s, 1H), 10.01 (s, 1H), 8.93 (s, 1H), 8.87 (d, J = 8.4 Hz, 1H), 8.84 (d, J = 8.4 Hz, 1H), 8.56 (d, J = 7.2 Hz, 1H), 8.56 (d, J = 7.6 Hz, 1H), 8.28 (d, J = 8.8 Hz, 2H), 7.92–7.85 (m, 4H), 7.75–7.70 (m, 2H), 7.66–7.61(m, 2H), 7.32 (d, J = 8.8 Hz, 2H), 5.36 (s, 2H), 3.12 (s, 2H), 2.30 (s, 6H); ^{13}C NMR (100 MHz, DMSO) δ 169.0, 158.9, 149.2, 143.5, 139.1, 136.9, 131.8, 127.7, 127.4, 127.0, 125.1, 124.9, 124.0, 123.6, 123.5, 122.7, 122.4, 121.8, 120.6, 120.3, 115.1, 63.2, 61.2, 45.3. ESI-HRMS m/z: calcd for $C_{34}H_{29}N_7O_2$ $[M + H]^+$ 568.2455, found 568.2469.

2.2.9. General procedure for the preparation of 21a–21f

The syntheses of **21a–21f** were carried out following procedures reported previously with minor modification [35]. To a solution of amine salt (30.8 mmol) in 30 mL water was added sodium azide (6.0 g, 92.3 mmol, 3 equiv.), and the mixture was stirred at 80 °C for 16 h. After removing most of the water by rotary evaporation, the reaction mixture was cooled in an ice bath. Diethyl ether (50 mL) and then KOH pellets (4.0 g) were added keeping the temperature below 10 °C.

After separation of the organic phase, the aqueous layer was further extracted with diethyl ether (2 × 20 mL). The combined organic layers were dried over Na_2SO_4 and concentrated to give oil products **21a**–**21f**, which were used directly for the next step reaction without further purification.

2.2.10. The syntheses of 22a–22f were carried out following the procedures for the syntheses of 19a–19d

2.2.10.1. 3-(4-((4-(1H-phenanthro[9,10-d]imidazol-2-yl)phenoxy) methyl)-1H-1,2,3-triazol-1-yl)propan-1-amine (22a). It was obtained with purity of 99% determined by using HPLC. ^{1}H NMR (400 MHz, DMSO) δ 8.95 (s, 2H), 8.49 (d, J = 5.2 Hz 1H), 8.37 (d, J = 4.8 Hz 1H), 8.30 (d, J = 8.0 Hz, 2H), 7.82 (d, J = 2.8 Hz, 2H), 7.82 (d, J = 2.4 Hz, 2H), 7.32 (d, J = 3.2 Hz, 2H), 5.31 (s, 2H), 4.48 (s, 2H), 2.62 (s, 2H), 2.03–1.89 (m, 2H); ^{13}C NMR (100 MHz, DMSO) δ 161.7, 160.5, 143.9, 142.2, 134.7, 128.7, 128.4, 128.4, 127.7, 127.7, 126.7, 126.4, 125.3, 124.7, 124.2, 124.0, 122.2, 120.4, 120.2, 119.4, 115.5, 61.4, 47.1. ESI-HRMS m/z: calcd for $C_{34}H_{29}N_7O_2$ $[M + H]^+$ 568.2455, found 568.2469.

2.2.10.2. 2-(4-((1-(2-(pyrrolidin-1-yl)ethyl)-1H-1,2,3-triazol-4-yl) methoxy)phenyl)-1H-phenanthro[9,10-d]imidazole (22b). It was obtained with purity of 99% determined by using HPLC. ^{1}H NMR (400 MHz, $CDCl_3$) δ 8.72 (t, J = 8.0 Hz, 2H), 8.60 (d, J = 8.0 Hz, 1H), 8.30 (d, J = 8.8 Hz, 3H), 7.79 (s, 1H), 7.75–7.64 (m, 4H), 7.16 (d, J = 8.8 Hz, 2H), 5.31 (s, 2H), 4.50 (t, J = 6.4 Hz, 2H), 2.97 (t, J = 6.4 Hz, 2H), 2.60–2.49 (m, 4H), 1.80–1.74 (m, 4H); ^{13}C NMR (100 MHz, $CDCl_3$) δ 162.1, 160.5, 144.5, 143.4, 135.5, 129.0, 128.9, 128.8, 127.3, 127.2, 126.2, 126.1 126.0, 123.7 123.4, 123.4, 122.9, 121.1, 120.7, 120.6, 115.2, 62.2, 55.4, 54.0, 49.5, 23.6. ESI-HRMS m/z: calcd for $C_{30}H_{28}N_5O_2$ $[M + H]^+$ 490.2238, found 490.2242.

2.2.10.3. 4-(2-(4-((4-(1H-phenanthro[9,10-d]imidazol-2-yl)phenoxy) methyl)-1H-1,2,3-triazol-1-yl)ethyl)morpholine (22c). It was obtained with purity of 96% determined by using HPLC. ^{1}H NMR (400 MHz, $CDCl_3$) δ 8.74 (t, J = 8.2 Hz, 2H), 8.61 (d, J = 7.6 Hz, 1H), 8.32 (d, J = 8.4 Hz, 3H), 7.79 (s, 1H), 7.76–7.65 (m, 4H), 7.17 (d, J = 8.4 Hz, 2H), 5.34 (s, 2H), 4.49 (t, J = 6.0 Hz, 2H), 3.68 (t, J = 7.8, 4H), 2.84 (t, J = 5.6 Hz, 2H), 2.49 (t, J = 4.4 Hz, 4H); ^{13}C NMR (100 MHz, $CDCl_3$) δ 162., 160.4, 144.6, 143.6, 135.6, 129.1, 128.9, 127.3, 127.2, 126.2, 126.0, 123.7, 123., 122.9, 121.1, 120.8, 120.7, 115.2, 66.8, 62.2, 57.8, 53.5, 47.5. ESI-HRMS m/z: calcd for $C_{30}H_{28}N_5O_3$ $[M + H]^+$ 506.2187, found 506.2190.

2.2.10.4. 2-(4-((4-(1H-phenanthro[9,10-d]imidazol-2-yl)phenoxy) methyl)-1H-1,2,3-triazol-1-yl)-N,N-diethylethanamine (22d). It was obtained with purity of 98% determined by using HPLC. ^{1}H NMR (400 MHz, $CDCl_3$) δ 8.73 (t, J = 8.2 Hz, 2H), 8.61 (d, J = 7.6 Hz, 1H), 8.30 (d, J = 8.8 Hz, 3H), 7.79 (s, 1H), 7.80–7.64 (m, 4H), 7.16 (d, J = 8.4 Hz, 2H), 5.32 (s, 2H), 4.42 (t, J = 6.0 Hz, 2H), 2.89 (t, J = 6.0 Hz, 2H), 2.54 (m, 4H), 0.96 (t, J = 7.2 Hz, 6H); ^{13}C NMR (100 MHz, $CDCl_3$) δ 162.2, 160.5, 144.6, 143.3, 135.6, 129.1, 128.9, 128.9, 127.3, 127.2, 126.2, 126.1, 126.0, 123.7, 123.7, 123.4 122.9, 121.1, 120.8, 120.7, 115.2, 62.2, 53.0, 49.2, 47.4 11.9. ESI-HRMS m/z: calcd for $C_{30}H_{30}N_5O_2$ $[M + H]^+$ 492.2394, found 492.2393.

2.2.10.5. 2-(4-((1-(2-(piperidin-1-yl)ethyl)-1H-1,2,3-triazol-4-yl) methoxy)phenyl)-1H-phenanthro[9,10-d]imidazole (22e). It was obtained with purity of 98% determined by using HPLC. ^{1}H NMR (400 MHz, $CDCl_3$) δ 8.73 (t, J = 8.0 Hz, 2H), 8.61 (d, J = 7.6 Hz, 1H), 8.31 (d, J = 8.4 Hz, 3H), 7.82 (s, 1H), 7.75–7.64 (m, 4H), 7.16 (d, J = 8.4 Hz, 2H), 5.32 (s, 2H), 4.47 (t, J = 6.2 Hz, 2H), 2.77 (t, J = 6.2 Hz, 2H), 2.42 (t, J = 6.2 Hz, 4H), 1.58–1.53 (m, 4H), 1.45–1.39 (m, 2H); ^{13}C NMR (100 MHz, $CDCl_3$) δ 162.2, 160.5, 144.6, 143.4, 135.5, 129.1, 128., 128.8, 127.3, 127.2, 126.2, 126.1, 126.0, 123.7, 123.5, 123.4, 122.9, 121.1, 120.8, 120.7, 115.2, 62.2, 58.2, 54.5, 47.9, 26.0, 24.1. ESI-HRMS m/z: calcd for $C_{31}H_{30}N_5O_2$ $[M + H]^+$ 504.2394, found 504.2392.

2.2.10.6. 3-(4-((4-(1H-phenanthro[9,10-d]imidazol-2-yl)phenoxy) methyl)-1H-1,2,3-triazol-1-yl)-N,N-dimethylpropan-1-amine (22f). It was obtained with purity of 99% determined by using HPLC. ^{1}H NMR (400 MHz, $CDCl_3$) δ 8.72 (t, J = 7.4 Hz, 2H), 8.60 (d, J = 7.4 Hz, 1H), 8.30 (d, J = 7.8 Hz, 3H), 7.77–7.63 (m, 5H), 7.15 (d, J = 8.0 Hz, 2H), 5.32 (s, 2H), 4.44 (t, J = 6.0 Hz, 2H), 2.26 (t, J = 6.0 Hz, 2H), 2.21 (s, 6H), 2.11–2.05 (m, 2H); ^{13}C NMR (100 MHz, $CDCl_3$) δ 162.1, 160.5, 144.6, 143.5, 135.6, 129.1, 128.9, 128.8, 127.3, 127.2, 126.2, 126.1, 126.0, 123.7, 123.4, 123.2, 122.9, 121.1, 120.8, 120.7, 115.2, 62.2, 55.7, 48.1, 45.2, 28.0. ESI-HRMS m/z: calcd for $C_{29}H_{28}N_5O_2$ $[M + H]^+$ 478.2238 found 478.2238.

2.3. Thioflavin T (ThT) assay

$A\beta_{1-42}$ (Sigma-Aldrich, USA) was dissolved in ammonium hydroxide (1% v/v) to give a stock solution (1 mM), which was aliquoted into small samples and stored at −80 °C. Thioflavin T (ThT) assay was performed to determine the activities of our compounds on inhibiting $A\beta_{1-42}$ self-aggregation. Experiments were performed by incubating the peptides ($A\beta_{1-42}$, 20 μM, final concentration) in 20 mM phosphate buffer (pH 7.4) at 37 °C for 48 h with the tested compounds (10 μM, final concentration). After incubation, the samples were diluted to a final volume of 40 μL with 50 mM glycine–NaOH buffer (pH 8.5) containing 5 μM thioflavin-T. Fluorescence signal was measured (excitation wavelength 450 nm, emission wavelength 485 nm, and slit widths set to 5 nm) on a monochromators based multimode microplate reader (INFINITE M1000), adapted for 384 well microtiter plates. Each inhibitor was examined in triplicate. The fluorescence intensities were recorded, and the percentage of inhibition on aggregation was calculated by using the following equation: $(1 - IF_i/IF_c) \times 100\%$ in which IF_i and IF_c were the fluorescence intensities obtained for absorbance in the presence and absence of inhibitors, respectively, after subtracting the background fluorescence of 5 μM thioflavin-T solution.

For the disaggregation of self-induced Aβ fibrils, the $A\beta_{1-42}$ stock solution was diluted with 20 mM phosphate buffer (pH 7.4). 20 μM $A\beta_{1-42}$ was incubated at 37 °C for 24 h. Then, the 20 μM tested compound was added and incubated at 37 °C for another 24 h. The sample was diluted to a final volume of 40 μL with 50 mM glycine–NaOH buffer (pH 8.0) containing thioflavin T (5 μM). The detection method was the same as above.

The effects of compounds on metal-induced $A\beta_{1-42}$ aggregation were also determined by using thioflavin T. The $A\beta_{1-42}$ stock solution was diluted with 20 μM HEPES (pH 6.6) containing 150 μM NaCl. 20 μM $A\beta_{1-42}$ was incubated with or without 20 μM copper or 20 μM iron and 20 μM tested compounds at 37 °C for 24 h. The sample was diluted to a final volume of 40 μL with 50 mM glycine–NaOH buffer (pH 8.0) containing thioflavin T (5 μM) and assayed as described above.

The inhibitory potency of compounds on AChE-induced $A\beta_{1-42}$ aggregation was determined by using thioflavin T. The mixtures containing 2 μL of $A\beta_{1-42}$ and 16 μL of AChE in the presence or absence of the tested compounds (2 μL) were incubated for 6 h at 37 °C. The final volume of each vial was 20 μL, and the final concentrations of $A\beta_{1-42}$ (diluted in 0.215 M sodium phosphate buffer, pH 8.0) and AChE (dissolved in 0.1 M sodium phosphate buffer, pH 8.0) were 25 μM and 0.25 μM. Blanks containing $A\beta_{1-42}$, AChE, $A\beta_{1-42}$ plus the tested compounds in 0.215 M sodium phosphate buffer were prepared. The percent inhibition on AChE-induced aggregation was calculated with the following equation: $(1 - IF_i/IF_c) \times 100\%$ where IF_i and IF_c were the fluorescence intensities obtained for $A\beta_{1-42}$ plus AChE in the presence and absence of inhibitors, respectively, minus the fluorescence of respective blanks.

2.4. Transmission electron microscope (TEM)

The $A\beta_{1-42}$ stock solution was diluted with 20 mM phosphate buffer (pH 7.4) for the metal free experiment and 20 μM HEPES (pH 6.6) including 150 μM NaCl for the copper and iron containing experiment. Then concentrations of $A\beta_{1-42}$, metal ions and tested compounds were 20 μM, 20 μM, and 40 μM, respectively. After incubation at 37 °C for 24 h, aliquots of 10 μL samples were placed on carbon-coated copper/rhodium grid. After 1 min, the grid was washed with water and negatively stained with 2% uranyl acetate solution for 1 min. After draining off the excess staining solution by filter paper, the specimen was transferred for examination in a transmission electron microscope (JEOL JEM-1400).

2.5. Inhibition studies on AChE and BuChE

Acetylcholinesterase (from electric eel), butyrylcholinesterase (from equine serum), 5,5′-dithiobis-(2-nitrobenzoic acid) (Ellman's reagent, DTNB), acetylthiocholine chloride (ATC), butylthiocholine chloride (BTC), and Tacrine hydrochloride were purchased from Sigma Aldrich.

The metal free assays were carried out in 0.1 M KH_2PO_4/K_2HPO_4 buffer (pH 8.0). Enzyme solutions were prepared by dissolving lyophilized powder in double-distilled water. Stock solutions of tested compounds (10 mM) were prepared in DMSO and diluted in phosphate buffer (pH 8.0). The assay solution (200 μL) consists of phosphate buffer (pH 8.0), with the addition of 10 μL of 0.01 M DTNB, 10 μL of enzyme, and 10 μL of 0.01 M substrate (ATC or BTC). Five increasing concentrations of inhibitors with their inhibitory activity ranged from 20% to 80% were added to the assay solution and pre-incubated for 10 min at 37 °C with the enzyme followed by the addition of corresponding substrate. Initial rate measurement assays were performed at 37 °C with a PowerWave XS2 microplate spectrophotometer. Absorbance value at 412 nm was recorded for 2 min, and the calculations were performed based on the method of Ellman et al. Each concentration was tested in triplicate, and IC_{50} values were calculated graphically from log concentration inhibition curve (Origin 7.5 software).

The determination of the inhibition effects on ChE in the presence of metal ions and $A\beta_{1-42}$ was carried out following the previously reported method. Compound **9g** was dissolved in HEPES buffer (pH 6.6) and one of the four conditions was followed. The assay solution was 200 μL. Condition (a): AChE or BuChE (0.08 U/mL final concentration) was added to the inhibitor solutions (100 μL) and incubated for 10 min. Then, the reactions were initialized with the addition of 10 μL of 0.01 M DTNB, and 10 μL of 0.01 M substrate (ATC or BTC). Condition (b): AChE or BuChE (0.08 U/mL final concentration) was added to the inhibitor solutions (100 μL) and incubated for 10 min. Then $CuSO_4$ or $FeSO_4$ or $A\beta_{1-42}$ peptide (10 μM) was added, and the mixture was incubated for another 10 min. The reactions were initialized with the addition of 10 μL of 0.01 M DTNB, and 10 μL of 0.01 M substrate (ATC or BTC). Condition (c): $CuSO_4$ or $FeSO_4$ or $A\beta_{1-42}$ peptide (10 μM) was added to the inhibitor solutions (100 μL) and incubated for 10 min. Then AChE or BuChE (0.08 U/mL final concentration) was added, and the mixture was incubated for another 10 min. The reactions were initialized with the addition of 10 μL of 0.01 M DTNB, and 10 μL of 0.01 M substrate (ATC or BTC). Condition (d): A mixture of AChE or BuChE (0.08 U/mL final concentration) and $CuSO_4$ or $FeSO_4$ or $A\beta_{1-42}$ peptide (10 μM) was added to the inhibitor solutions (100 μL) and incubated for 10 min. The reactions were initialized with the addition of 10 μL of 0.01 M DTNB, and 10 μL of 0.01 M substrate (ATC or BTC).

2.6. Kinetic characterization of AChE inhibition

Kinetic characterization of AChE inhibition was performed based on a reported method. The assay solution (200 μL) consists of 0.1 M phosphate buffer (pH 8.0), with the addition of 10 μL of 0.01 M DTNB, 10 μL of enzyme, and 10 μL of substrate (ATC). Four different concentrations of inhibitors were added to the assay solution and pre-incubated for 10 min at 37 °C with the enzyme followed by the addition of substrate in different concentrations. Kinetic characterization for the hydrolysis of ATC catalyzed by AChE was carried out using spectrometric method at 412 nm. The parallel control experiments were performed without inhibitor in the assay.

2.7. Anti-oxidation activity with in vitro-ORAC-FL assay

The anti-oxidation activity was determined based on the oxygen radical absorbance capacity-fluorescein (ORAC-FL) assay. The reaction was carried out in 75 mM potassium phosphate buffer (pH 7.4), and the final volume of reaction mixture was 200 μL. The tested compound or Trolox standard substance was dissolved in DMSO to 10 mM and diluted in 75 mM potassium phosphate buffer (pH 7.4). Antioxidant (20 μL) and fluorescein (FL, 120 μL, final concentration of 140 nM) were incubated for 15 min at 37 °C placing in the wells of a black 96 well plate. Then 60 μL of 2,2′-azobis(amidinopropane) dihydrochloride (AAPH, final concentration of 40 mM) solution was added rapidly. The fluorescence was recorded every minute for 240 min at 485 nm (excitation wavelength) and 535 nm (emission wavelength). The final concentration of tested compound or Trolox standard substance was 1–5 μM. A blank (FL + AAPH in 75 mM potassium phosphate buffer) instead of the sample and Trolox calibration solution was used in each assay. All the reactions were carried out in triplicate, and each reaction was repeated for at least three times. Anti-oxidation curves (fluorescence versus time) were normalized to the curve of the blank in the same assay, and then the area under the fluorescence decay curve (AUC) was calculated. The net AUC of a sample was obtained by subtracting the AUC of the blank. ORAC-FL values were expressed as Trolox equivalents by using the standard curve calculated for each sample, where the ORAC-FL value of Trolox was taken as 1, indicating the anti-oxidative potency of the tested compounds.

2.8. Anti-oxidation activity in SH-SY5Y cells

Intracellular ROS were measured with the a fluorescent probe (2′,7′-dichlorofluorescein diacetate, DCFH-DA) as reported with some variation. Human neuroblastoma cells, SH-SY5Y, were routinely grown at 37 °C in a humidified incubator with 5% CO_2 in Dulbecco's modified Eagle's medium (DMEM, GIBCO) containing 15 nonessential amino acid and supplemented with 10% fetal calf serum (FCS, GIBCO), 1 mM glutamine, 50 mg/μL penicillin, and 50 mg/μL streptomycin. For assays, SH-SY5Y cells were sub-cultured in 96-well plates at a seeding density of 3×10^4 cells per well. After 24 h, the cells were treated with the synthesized compounds at concentrations of 3.125 μM, 6.25 μM, 12.5 μM, and 25 μM. Trolox was used as a reference compound. After 24 h of treatment with the compounds, the cells were washed with phosphate buffer, and then incubated with 5 μM DCFH-DA in phosphate buffer at 37 °C in 5% CO_2 for 30 min. After DCFH-DA was removed, the cells were washed and incubated with 0.1 mM *t*-BuOOH in phosphate buffer for 30 min. At the end of the incubation, the fluorescence of the cells from each well was measured at 485 nm excitation and 535 nm emission with a monochromators based multimode microplate reader (INFINITE M1000). Results are expressed as a percentage of the sample average divided by the control group data, calculated as follows: $(OD_{sample} - OD_{blank})/(OD_{control} - OD_{blank}) \times 100\%$.

2.9. Metal-chelating study

The chelating studies were made in buffer (20 mM HEPES, 150 mM NaCl, pH 7.4) using a UV–vis spectrophotometer (SHIMADZC UV-2450PC). The absorption spectra of compound **9g** (20 μM), alone or in the presence of $CuSO_4$, $FeSO_4$, and $ZnCl_2$ (40 μM), were recorded at room temperature in a 1 cm quartz cell.

2.10. Cell culture and MTT assay

Cytotoxicity was evaluated with the colorimetric MTT [3-(4,5-dimethyl-2-thiazolyl)-2,5-diphenyl-2H-tetrazolium bromide] assay. SH-SY5Y cells were sub-cultured in 96-well plates at a seeding density of 10,000 cells per well. After 24 h, the cells were treated with different concentrations of compounds (0–50 μM). After 48 h, the survival of cells was determined with MTT assay. Briefly, 20 μL of MTT (5 mg/mL) was added to each well and incubated for 4 h. The MTT medium in each well was carefully removed and 100 μL DMSO was added into each well, followed by incubation at 37 °C for 10 min with horizontal shaking. The absorbance of each well was measured with a micro culture plate reader at the wavelength of 570 nm. The IC_{50} values were calculated graphically from log concentration–inhibition curve (Origin 7.5 software).

2.11. Determination of neuroprotective activity

$A\beta_{1-42}$ was dissolved to 10 mM with DMSO and further diluted into 100 μL of 40, 20, and 10 μM, with Dulbecco's modified Eagle's medium, respectively. DMSO was added to 100 μL Dulbecco's modified Eagle's medium to give the blank control. Then the $A\beta_{1-42}$ of 40, 20, 10 μM and the blank control were pre-incubated for 48 h for aging fibrils at 37 °C (as prepared in aggregation studies). Aggregated $A\beta_{1-42}$ (40, 20, 10 μM) were added to the SH-SY5Y cells, which had been incubated for 24 h. Absorbance value was measured at 570 nm through MTT methods. To study the protective effect of **9g** on the neurotoxicity of $A\beta_{1-42}$, 20 μM $A\beta_{1-42}$ seed samples, with or without **9g** (3.125–12.5 μM), were pre-incubated at 37 °C for 48 h. Then the prepared samples were added to SH-SY5Y cells, and incubated at 37 °C for 48 h. DMSO diluted with phosphate buffer solution was also added to the blank control wells. The final concentration of DMSO in each well was less than 0.5%. At the end of the experiment, samples were tested via MTT methods. Absorbance value was measured to determine cell viability.

2.12. Dot blot assays

Dot blot assays to detect $A\beta_{1-42}$ fibril aggregation with B10 were performed as described previously with minor modification [36]. Briefly, $A\beta_{1-42}$ was diluted into 20 μM with buffer (20 mM HEPES, 150 mM NaCl, pH 7.4) and then incubated with or without $CuSO_4$ or $FeSO_4$ (20 μM), and the concentrations of **9g** were 20 μM and 40 μM. After incubation at 37 °C for 24 h, 10 μL aliquots of 20 μM $A\beta_{1-42}$ reactions were spotted onto nitrocellulose membranes. Membranes were blocked for 2 h with 10% non-fat milk in TBS. After washing, membranes were incubated with the anti-Aβ fibril antibody (1:2000 dilution) dissolved in TBS containing 3% BSA and 0.01% Tween-20 and developed using an alkaline-phosphatase antirabbit secondary antibody (1:5000 dilution). Invitrogen's Western Breeze Chemiluminescent kit was used to visualize the protein dots, and these dots were imaged using a FUJIFILM Luminescent Image Analyzer LAS-1000CH.

2.13. Native gel electrophoresis and Western blot

Gel electrophoresis and Western blot [37] were performed to determine the inhibition of $A\beta_{1-42}$ aggregation by **9g** in the presence or absence of metal ions with antibody 6E10. The preparation of samples were the same as that for ThT assay, and 20 μM $A\beta_{1-42}$ was incubated with various concentrations of **9g** (20 μM, 40 μM) in the presence or absence of 20 μM $CuSO_4$ or $FeSO_4$ at 37 °C for 24 h. Samples were separated on 10–20% gradient Tris–tricine mini gels. The gel was transferred to a nitrocellulose membrane in an ice bath, and the protocol was followed as suggested except that the membrane was blocked for 2 h with 10% non-fat milk in TBS. After blocking, the membrane was incubated in a solution (1:2000 dilution) of 6E10 anti-Aβ primary antibody (Covance) for 2 h, and developed using an alkaline-phosphatase antimouse secondary antibody (1:5000 dilution). Invitrogen's Western Breeze Chemiluminescent kit was used to visualize the protein bands, and these bands were imaged using a FUJIFILM Luminescent Image Analyzer LAS-1000CH.

2.14. CD spectroscopy

The secondary structure of $A\beta_{1-42}$ aggregates was evaluated using a Jasco-810-150S spectropolarimeter (Jasco, Japan) at room temperature as described previously [38]. $A\beta_{1-42}$ (20 μM) was mixed with and without 10, 20 μM **9g** in 20 mM sodium phosphate buffer (pH 7.4). All solutions were incubated at 37 °C for 48 h. Spectra were recorded at 25 °C between 190 and 260 nm with a band width of 0.5 nm, a 3 s response time, and scan speed of 10 nm/min. Background spectra and when applicable, spectra of **9g** were subtracted.

2.15. Molecular docking study

The crystal structure of human AChE (PDB ID: 1B41, resolution = 2.76 Å) was retrieved from the Protein Data Bank. For docking study, short peptide and water molecules were removed. The apo structure was superposed with the co-crystal structure of Torpedo californica AChE and F11 (PDB ID: 2CMF [39], resolution = 2.5 Å), and then the complex of human AChE and F11 was kept. The complex was prepared in the"Protein Preparation Wizard" workflow in Maestro, version 9.4 [40], and bond orders were assigned. All the heavy atoms were minimized to reach the converge root mean square deviation (RMSD) of 0.30 Å with the OPLS_2005 force field. After preparation, the docking grid was generated using "Receptor Grid Generation", the grid enclosing box was centered on the original ligand (F11) a size of $10 \times 8 \times 10$ ($x \times y \times z$, Å), and a scaling factor of 0.80 was set to van der Waals radii of those receptor atoms with a partial atomic charge less than 0.15. Compound **9g** was optimized using MMFF force field [41] and the Powell method was used for energy minimization by default parameters in Discovery studio 2.5 (Accelrys Inc.). Extra precision mode (Glide XP) was employed for identifying the potential binding of compound **9g** to the human AChE.

The initial coordinates of human BuChE used in our computational studies came from the X-ray crystal structure (PDB ID: 1POP) [42]. The missing residues (D2, D3, E255, D378, D379, N455, L530, E531, and M532) were built using the automated homology modeling tools in Discovery Studio 2.5. The binding site was defined as a box with the center of the native ligand. Extra precision mode (Glide XP) was applied for identifying the potential binding of compound **9g** to the BuChE with the default parameters.

For $A\beta_{1-42}$ docking study, the initial structure of $A\beta_{1-42}$ was taken from the NMR structure (PDB ID: 1IYT) [43]. Autodock 4.0 was employed to identify the binding poses of **9g** for $A\beta_{1-42}$ with a Lamarckian genetic algorithm [44]. The grid map, with $80 \times 80 \times 80$ points spaced equally at 0.375 Å, was generated using the Auto Grid program to evaluate the binding energies between ligand and receptor. All docked poses of compound **9g** were clustered using a tolerance of 2 Å for the RMSD and ranked on the basis of the binding docking energies, and the lowest energy conformation in the most populated cluster was chosen for further study.

3. Results and discussion

3.1. Organic syntheses of imidazole derivatives

Compounds **7a–9f**, **7g–9g**, **19a–20e**, **22a–22f** were synthesized as described in Schemes 1–4. As shown in Scheme 1, commercially available 4-hydroxybenzaldehyde was first reacted with 1,2-dibromoethane, 1,3-dibromopropane, or 1,4-dibromobutane to give product **1**, **2**, or **3**, respectively. The product **1**, **2**, or **3** was reacted with phenanthrene-9,10-

dione to produce intermediate **4**, **5**, or **6**, which was then reacted with various amines to give final products **7a–9f**. In Scheme 2, the intermediate **4**, **5**, or **6** was used to react with pyridine to produce **7g**, **8g**, and **9g**. Similarly, as shown in Scheme 3, 4-hydroxybenzaldehyde was first reacted with propargyl bromide, followed with phenanthrene-9,10-dione to give intermediate **11**. The syntheses of **12a–12b**, **13a–13d**, **14a–14e**, **15a–15d**, **16a–16e**, **17a–17d**, and **18a–18e** were carried out by following the procedures reported previously [45–47]. The intermediate **11** was then reacted with **17a–18e** through "click" chemistry with introduction of triazole rings to afford products **19a–20e** [45–48]. The intermediate **11** was also reacted with azide **21a–21f** to give products **22a–22f** as shown in Scheme 4.

3.2. Inhibition of self-mediated $A\beta_{1-42}$ aggregation

The inhibition of self-mediated $A\beta_{1-42}$ aggregation by our synthesized imidazole derivatives were studied by using thioflavin T (ThT) assay [49] with resveratrol as a reference compound. The effects of these compounds on $A\beta_{1-42}$ peptide aggregation at concentration of 10 μM and the IC_{50} of these compounds against self-mediated $A\beta_{1-42}$ aggregation were summarized as shown in Table 1. The IC_{50} value of resveratrol against $A\beta_{1-42}$ aggregation was 10 μM, in comparison, more than half of our compounds displayed better inhibition effects than resveratrol. The first series of our compounds **7a–9g** almost all showed more than 50% inhibition effect except **7f** with 28% inhibitory activity when used at 10 μM concentration. Compound **9g** was found to have 74% $A\beta_{1-42}$ aggregation inhibitory effect when used at 10 μM concentration with its IC_{50} value of 6.5 μM. The compounds with incorporation of triazole rings also displayed some inhibitory activity from 13% to 71% for $A\beta_{1-42}$ aggregation when used at 10 μM concentration, and the IC_{50} value of **19a** against $A\beta_{1-42}$ aggregation was 6.7 μM. The reason of the similarities of anti-$A\beta_{1-42}$ aggregation activity of our compounds were explored by using molecular docking experiment and the scores of the representative compounds **9d, 19a**, **22e**, and **9g** were −3.9514, −4.8855, −4.2690, −4.6432, respectively, and the binding modes of these compounds with $A\beta_{1-42}$ were similar (Fig. 3S).

3.3. Inhibition studies for AChE and BuChE

The inhibitory activity of our synthetic derivatives was evaluated against AChE and BuChE using the method of Ellman et al. [50] with Tacrine as a positive control. AChE from *electric eel* and BuChE from *equine serum* were used in this study because of their high sequence homology to the human enzymes. As shown in Table S1, our most synthesized imidazole derivatives displayed strong inhibitory activity to ChE at micromole level, which were weaker than Tacrine. Compound **9g** had potent inhibitory activity for both AChE and BuChE with its IC_{50} values of 860 nM and 510 nM for AChE and BuChE, respectively, which were much better than those reported previously for other imidazole derivatives [32,33]. The Lineweaver Burk plots showed a mixed-type inhibition of **9g** to AChE (Fig. S1), indicating that **9g** could bind to both catalytic active site (CAS) and peripheral anionic site (PAS) of AChE. The expanded aromatic plane and the pyridine moiety at the end of the chain facilitated the binding of **9g** to the ChE, which is consistent with our following molecular modeling studies.

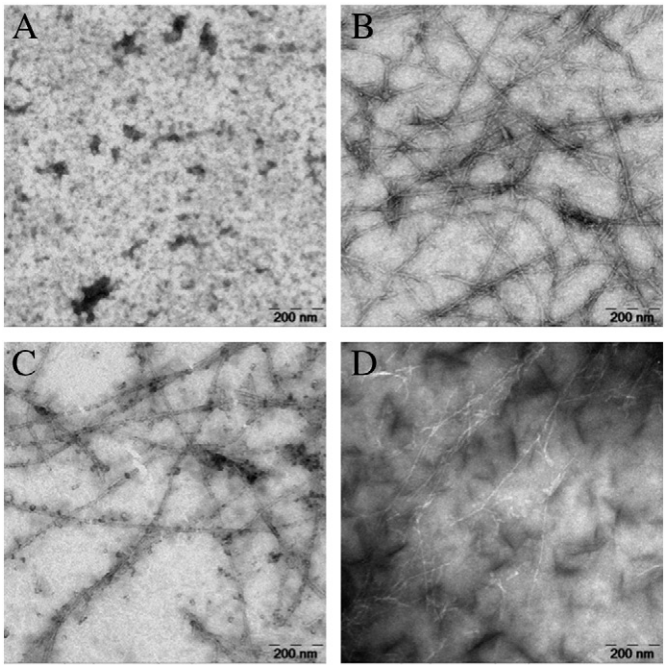

Fig. 1. TEM image analysis of $A\beta_{1-42}$ aggregation in the presence of **9g**. (A) $A\beta_{1-42}$ (20 μM), 0 h. (B) $A\beta_{1-42}$ (20 μM) alone was incubated at 37 °C for 24 h. (C) $A\beta_{1-42}$ (20 μM) and resveratrol (20 μM) were incubated at 37 °C for 24 h. (D) $A\beta_{1-42}$ (20 μM) and **9g** (20 μM) were incubated at 37 °C for 24 h.

Table 1
Effects of our compounds on $A\beta_{1-42}$ aggregation.

Compound	$A\beta_{1-42}$ aggregation inhibition (%)[a]	$A\beta_{1-42}$ IC_{50} (μM)[b]	Compound	$A\beta_{1-42}$ aggregation inhibition (%)	$A\beta_{1-42}$ IC_{50} (μM)
7a	51 ± 3	8.9 ± 0.2	**9f**	70 ± 2	7.0 ± 0.8
7b	65 ± 1	7.9 ± 0.4	**g**	74 ± 2	6.5 ± 0.4
7c	54 ± 1	9.2 ± 0.3	**19a**	71 ± 1	6.7 ± 0.4
7d	77 ± 1	7.0 ± 0.6	**19b**	63 ± 4	8.0 ± 1.2
7e	62 ± 1	8.0 ± 0.1	**19c**	13 ± 1	n.d.
7f	28 ± 3	n.d.[c]	**19d**	58 ± 4	7.5 ± 1.2
7 g	55 ± 1	9.0 ± 0.4	**20a**	60 ± 3	8.6 ± 2.2
8a	55 ± 1	9.7 ± 0.7	**20b**	51 ± 1	10.0 ± 1.1
8b	56 ± 5	9.2 ± 1.2	**20c**	50 ± 1	n.d.
8c	59 ± 3	9.0 ± 1.0	**20d**	55 ± 2	8.4 ± 0.3
8d	61 ± 3	7.9 ± 1.5	**20e**	65 ± 3	7.4 ± 0.8
8e	72 ± 7	7.0 ± 0.8	**22a**	41 ± 6	n.d.
8f	60 ± 2	8.5 ± 2.2	**22b**	23 ± 3	n.d.
8 g	64 ± 4	7.4 ± 1.4	**22c**	35 ± 2	n.d.
9a	58 ± 8	8.5 ± 2.1	**22d**	57 ± 3	9.0 ± 1.0
9b	68 ± 2	8.3 ± 0.3	**22e**	24 ± 4	n.d.
9c	72 ± 5	7.3 ± 0.6	**22f**	54 ± 2	8.4 ± 0.6
9d	73 ± 4	7.0 ± 1.0	**Resveratrol**	53 ± 2	10.0 ± 0.6
9e	52 ± 2	9.8 ± 1.1			

[a] The thioflavin-T fluorescence method was used. The values are expressed as the mean ± SD of at least three independent measurements. All values were obtained at a compound concentration of 10 μM.
[b] The IC_{50} (μM) values shown are the mean ± SD of three experiments.
[c] n.d. means not determined.

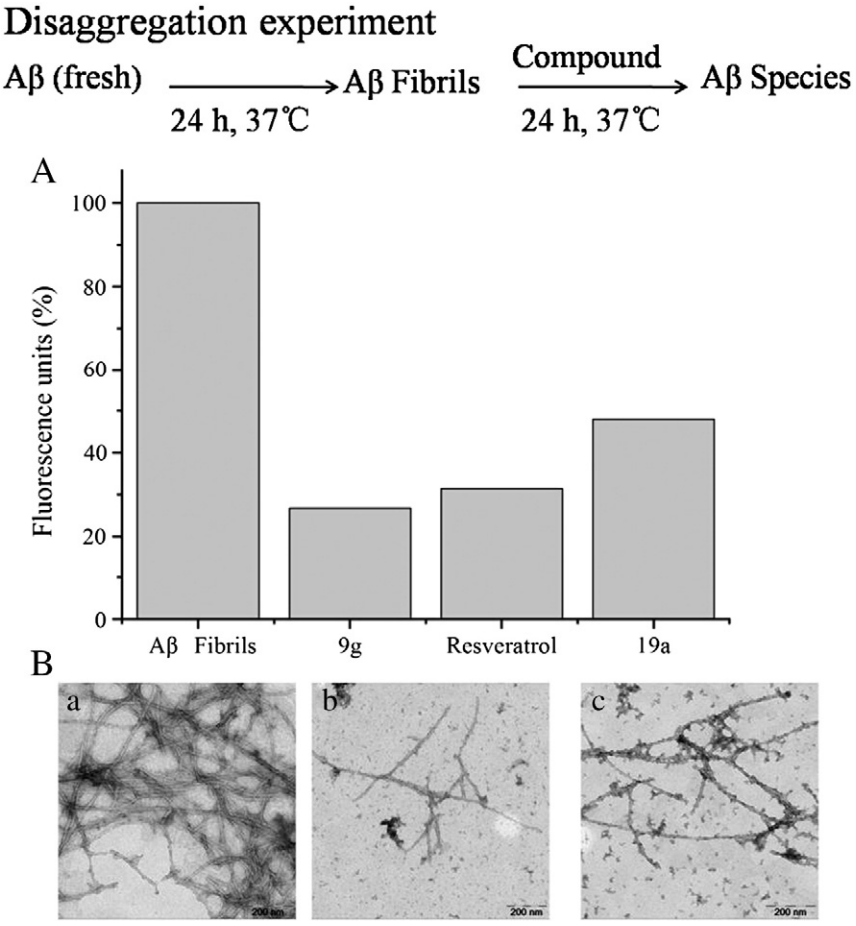

Fig. 2. Disaggregation experimental result. (A) ThT binding assay for Aβ_{1-42} without and with test compound. (B) TEM images for Aβ_{1-42} disaggregation. (a) Aβ_{1-42} (20 μM) was incubated at 37 °C for 24 h in phosphate buffer. (b) Aβ_{1-42} (20 μM) was incubated with **9g** (20 μM) at 37 °C for 24 h. (c) Aβ_{1-42} (20 μM) was incubated with resveratrol (20 μM) at 37 °C for 24 h.

3.4. Anti-oxidation activity studies

The reduction of the oxidative stress is another crucial aspect in designing agents for AD treatment. The anti-oxidation activities of the imidazole derivatives have been studied by using the oxygen radical absorbance capacity assay method with fluorescein (ORAC-FL) [51,52], and vitamin E analogue Trolox has been used as a standard. We studied our compounds for anti-oxidation activity with this assay method, and

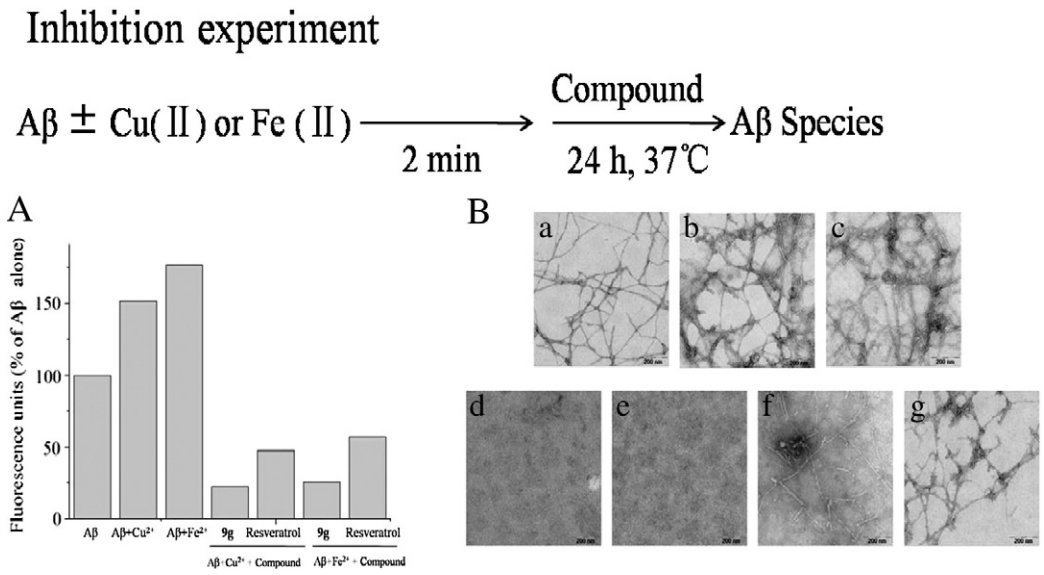

Fig. 3. Metal induced Aβ aggregation was carried out with incubation for 2 min, followed with test compound induced Aβ disaggregation upon incubation at 37 °C for 24 h. (A) ThT binding assay for metal induced Aβ aggregation, and test compound induced Aβ disaggregation. (B) TEM images for metal induced Aβ aggregation, and test compound induced Aβ disaggregation. The incubations were carried out with following reagents: (a) 20 μM Aβ_{1-42} alone. (b) 20 μM Aβ_{1-42} and 20 μM Cu^{2+}. (c) 20 μM Aβ_{1-42} and 20 μM Fe^{2+}. (d) 20 μM Aβ_{1-42}, 20 μM Cu^{2+}, and 40 μM **9g**. (e) 20 μM Aβ_{1-42}, 20 μM Fe^{2+}, and 40 μM **9g**. (f) 20 μM Aβ_{1-42}, 20 μM Cu^{2+}, and 40 μM resveratrol. (g) 20 μM Aβ_{1-42}, 20 μM Fe^{2+}, and 40 μM resveratrol.

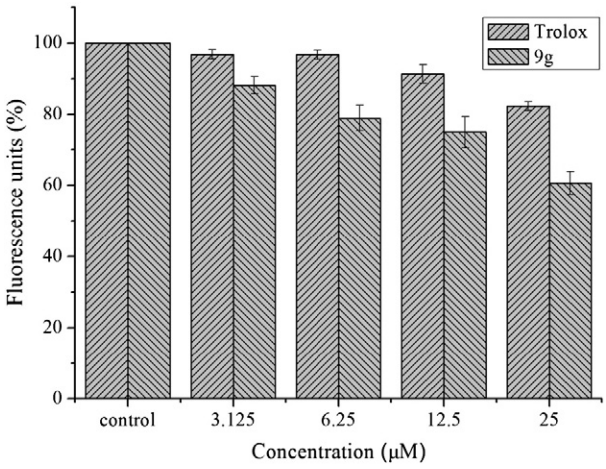

Fig. 4. Percentage increase in intracellular ROS induced by exposure to *t*-BuOOH, as determined by DCFH-DA. The concentrations of compounds were 3.125 μM, 6.25 μM, 12.5 μM, and 25 μM.

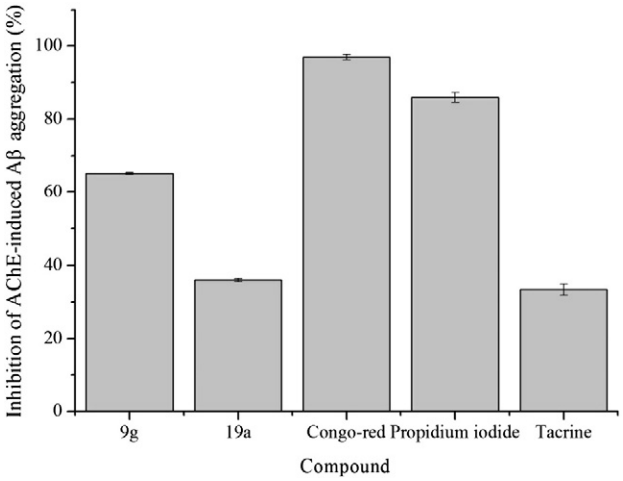

Fig. 6. The inhibitory activity of our imidazole derivatives to AChE-induced Aβ_{1-42} aggregation. The concentration of Aβ_{1-42} was 25 μM, and the concentration ratio of Aβ_{1-42}, AChE, compound was 100:1:100.

found that most of our compounds showed relatively low ORAC-FL values compared to Trolox, as shown in Table S1. In comparison, compound **9g** displayed relatively high anti-oxidation activity, with approximately 2.29 times higher activity than Trolox when used at 5 μM concentration. The anti-oxidation mechanism of **9g** is not clear at this time. We think that **9g** could have several possible mechanisms for its anti-oxidation activity in cells. The core structure of phenanthroimidazole is somehow similar to that of melatonin, a well-known anti-oxidation agent, which could prevent the generation of ROS through its interaction with intracellular superoxide anion. Besides, **9g** may play an indirect anti-oxidation role through activation of some anti-oxidation enzymes in cells. In addition, higher concentration of metal ions could cause increased ROS, and **9g** could reduce the generation of ROS through metal chelation.

3.5. Cytotoxic studies on SH-SY5Y neuroblastoma cells

The cytotoxicity of our imidazole derivatives to the human neuroblastoma SH-SY5Y cells was evaluated by using colorimetric MTT assay. The cells were treated with various concentrations of compounds for 48 h with maximum concentration of 50 μM. As shown in Table 1, most compounds showed their IC_{50} values of more than 10 μM, indicating their low neural cytotoxic effects. Compound **9g** had its IC_{50} value of more than 50 μM, indicating its very low neural cytotoxicity. As mentioned above, considering that compound **9g** inhibited 74% Aβ_{1-42} aggregation, and had its IC_{50} values of 860 nM and 510 nM for AChE and BuChE respectively, with 2.29 times higher anti-oxidation activity than Trolox and very low cytotoxic effect to neural cells, this compound could become a promising lead compound for further development for AD treatment.

3.6. Inhibition of Aβ_{1-42} fibril formation monitored by using transmission electron microscopy (TEM)

To further study the activity of compound **9g** for its inhibition of Aβ_{1-42} aggregation, its inhibitory activity was monitored by using transmission electron microscopy (TEM) [53], with resveratrol as a reference compound. After 24 h of incubation at 37 °C, Aβ_{1-42} alone aggregated into well-defined Aβ fibrils (Fig. 1B). In contrast, few and slender Aβ fibrils were observed in the presence of compound **9g** (Fig. 1D) under identical conditions. Therefore, based on the TEM and ThT measurement results, we can conclude that compound **9g** could effectively inhibit Aβ_{1-42} fibril formation.

3.7. Disaggregation of self-induced Aβ_{1-42} aggregation fibrils by 9g

The ability of **9g** to disaggregate self-induced Aβ_{1-42} aggregation fibrils was investigated. Aβ_{1-42} fibrils were generated by incubating fresh Aβ_{1-42} for 24 h at 37 °C. The test compound was then added to

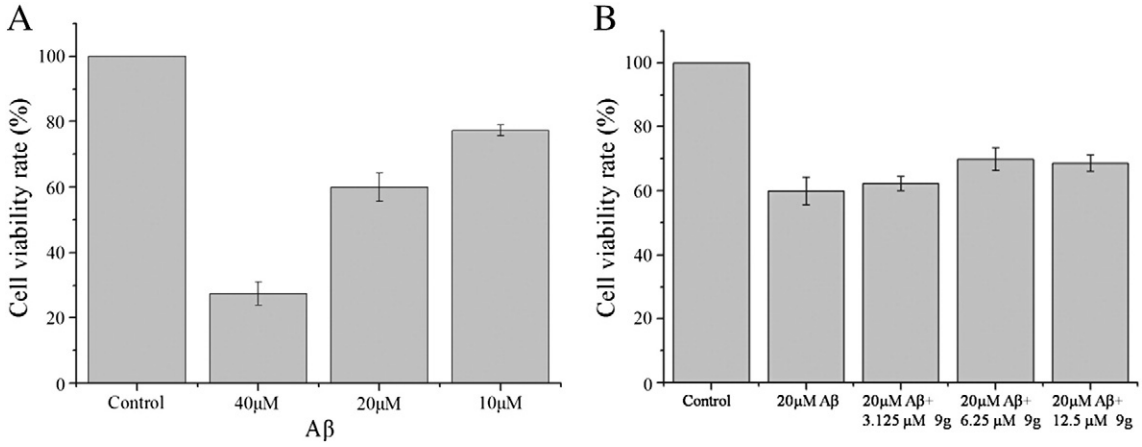

Fig. 5. Protective effect of **9g** on Aβ_{1-42}-induced toxicity in SH-SY5Y cell lines. (A) Aβ_{1-42} (10, 20 and 40 μM) were incubated with SH-SY5Y cells for 48 h. (B) Aβ_{1-42} (20 μM) was incubated with SH-SY5Y cells in the absence or presence of various concentrations of **9g** for 48 h. Cell viability was determined by using MTT methods.

Table 2
IC_{50} values for inhibition of ChE by compound **9g** in HEPES buffer (nM).

IC_{50} (nM)						
	AChE			BuChE		
Experiment	$CuSO_4$	$FeSO_4$	$A\beta_{1-42}$	$CuSO_4$	$FeSO_4$	$A\beta_{1-42}$
a	796	796	796	495	495	495
b	820	845	903	527	478	493
c	766	642	800	445	483	511
d	753	822	829	400	367	515

Experiments: (a) **9g** was incubated with AChE (or BuchE) for 10 min. (b) **9g** was incubated with AChE (or BuchE) for 10 min, followed with addition of Cu^{2+} or Fe^{2+} or $A\beta_{1-42}$ and incubation of the mixture for additional 10 min. (c) **9g** was incubated with Cu^{2+} or Fe^{2+} or $A\beta_{1-42}$ for 10 min, followed with addition of AChE (or BuChE) and incubation of the mixture for additional 10 min. (d) AChE (or BuChE) was incubated with Cu^{2+} or Fe^{2+} or $A\beta_{1-42}$ for 10 min, followed with addition of **9g** and incubation of the mixture for additional 10 min.

the sample and incubated for another 24 h at 37 °C. Our ThT binding assay result showed that compound **9g**, resveratrol, and compound **19a** could all disaggregate $A\beta_{1-42}$ fibrils at 20 μM concentration with ratio of 73.3%, 68.7%, and 52%, respectively, as shown in Fig. 2(A). Our TEM result further demonstrated the disaggregation effect of compound **9g** in comparison with resveratrol, as shown in Fig. 2(B).

3.8. Effect of 9g on metal-induced $A\beta_{1-42}$ aggregation

Transition metal ions, especially Cu, Fe, Zn, play important role in the development of AD. The interaction of **9g** with Cu(II), Fe(II), and Zn(II) was studied by using UV–vis spectroscopy [37,54,55]. As shown in Fig. S2, the addition of 2 equivalents of metal ions to 20 μM **9g** caused decreased UV absorbance for **9g**, indicating the interaction of metal ions with **9g**.

To investigate the ability of our imidazole derivatives to inhibit metal-induced Aβ aggregation, we studied the effect of **9g** on metal-induced $A\beta_{1-42}$ aggregation by ThT fluorescence and TEM. After incubation at 37 °C for 24 h, Cu^{2+} and Fe^{2+} could induce the fibrillization of $A\beta_{1-42}$ at the levels of 151.6% and 176.9%, respectively, in comparison with the fibrillization of $A\beta_{1-42}$ alone as 100%. More fibrils could be observed with the TEM (Fig. 3b and c). The addition of **9g** could significantly reverse these effects, rescuing 129.5% and 151.4% $A\beta_{1-42}$ aggregation induced by Cu^{2+} and Fe^{2+} respectively, and its disaggregation effect was better than resveratrol (rescuing 104.0% aggregation induced by Cu^{2+}, and 120.0% aggregation induced by Fe^{2+}). These disaggregation effects were consistent with our TEM image results, and we could barely see the fibrils for **9g**-treated $A\beta_{1-42}$ (Fig. 3d and e).

3.9. Anti-oxidation activity of 9g in SH-SY5Y cells

The ability of **9g** to counteract the formation of ROS was assayed in human neuroblastoma cells (SH-SY5Y) based on dichlorofluorescein diacetate (DCFH-DA), after the treatment with *tert*-butyl hydroperoxide (*t*-BuOOH), a compound used to induce oxidative stress [56,57]. Trolox was used as a reference control compound. The concentrations of tested compounds were 3.125 μM, 6.25 μM, 12.5 μM, and 25 μM. As shown in Fig. 4, both Trolox and compound **9g** exhibited dose-dependent antioxidant activity, and the activity of **9g** was higher than that of Trolox.

3.10. Compound 9g protects cells against $A\beta_{1-42}$-induced toxicity

As mentioned before, compound **9g** had low cell toxicity, with its IC_{50} value of more than 50 μM for SH-SY5Y cells. The neuroprotective activity of **9g** was further studied following a procedure reported previously with minor modification [58]. SH-SY5Y cells were treated with $A\beta_{1-42}$ solutions at 10 μM, 20 μM, and 40 μM concentrations. $A\beta_{1-42}$-induced cytotoxicity was determined as shown in Fig. 5a, which indicated that $A\beta_{1-42}$ significantly reduced cell viability in a dose-dependent manner. It was found that the cells were well protected when 20 μM $A\beta_{1-42}$ was mixed with compound **9g** at 3.125 μM, 6.25 μM, and 12.5 μM concentrations, as shown in Fig. 5b. This result showed that **9g** was a neuroprotective agent against $A\beta_{1-42}$-induced toxicity at low concentration.

3.11. Inhibition of 9g on AChE-induced $A\beta_{1-42}$ aggregation

It has been reported that Aβ deposition in AD brain is linked to AChE expression, and the PAS of AChE can bind to the Aβ, accelerating the formation of amyloid fibrils [59,60]. The inhibitory activity of our imidazole derivatives to AChE-induced $A\beta_{1-42}$ aggregation was also determined by using thioflavin T (ThT) assay, with Tacrine, propidium iodide, and Congo-red as reference compounds. As shown in Fig. 6, Tacrine, with its high affinity for CAS rather than PAS of AChE, showed 33.4% inhibitory effect against AChE-induced $A\beta_{1-42}$ aggregation. In comparison, propidium iodide significantly reduced about 85.9% $A\beta_{1-42}$ aggregation as a result of its noncompetitive inhibition type. Our imidazole derivatives **9g** and **19a** displayed 65.2% and 36.0% inhibition of ChE-induced $A\beta_{1-42}$ aggregation, respectively. Compound **9g** was better than the single site inhibitor Tacrine, indicating its possible dual binding effect to AChE with mixed type inhibitory activity.

3.12. Effects of metal ions and $A\beta_{1-42}$ on inhibition of ChE by compound 9g

It is possible that Aβ and metal ions could interact with compound **9g**, which could prevent the binding of **9g** with ChE. Therefore, the

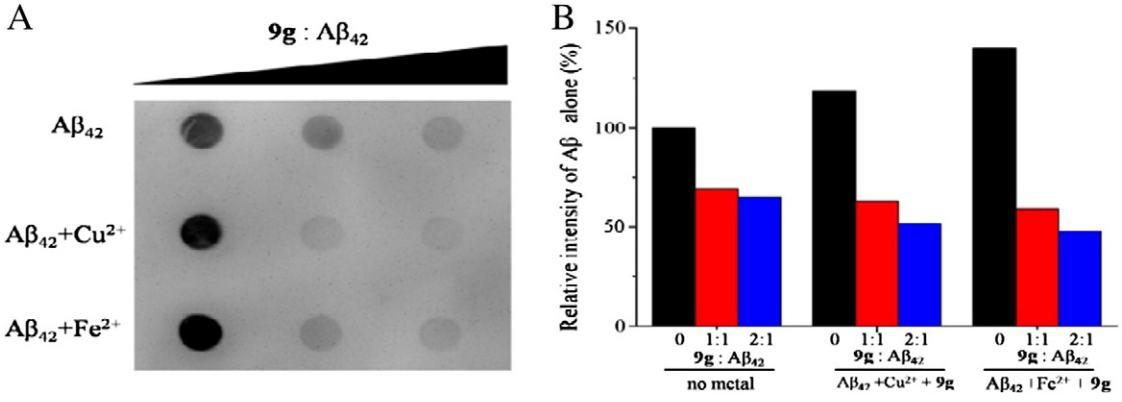

Fig. 7. Dot plot analysis for the inhibition of self-aggregation and metal-induced formation of Aβ fibrils by **9g** with Aβ fibrils antibody B10. The concentrations of $A\beta_{1-42}$ and metal ions were 20 μM, and the concentrations of **9g** were 20 μM and 40 μM. (A) Dot plot image of $A\beta_{1-42}$ in the presence or absence of metal ions and/or **9g** after incubation at 37 °C for 24 h. (B) Bar graphical analysis for the relative intensity of the dot plot result.

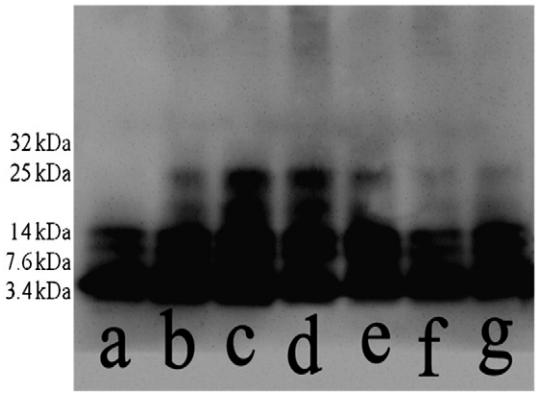

Fig. 8. Gel electrophoresis and Western blot analysis for the inhibition of $A\beta_{1-42}$ aggregation by **9g** in the presence or absence of metal ions with antibody 6E10. $A\beta_{1-42}$ used was 20 μM, the metal ions used was 20 μM, and the concentrations of **9g** were 20 μM and 40 μM for the inhibition of $A\beta_{1-42}$ aggregation and 40 μM for the inhibition of metal-induced $A\beta_{1-42}$ aggregation. (a) Incubation of $A\beta_{1-42}$ alone for 24 h at 37 °C. (b) Incubation of $A\beta_{1-42}$ with 20 μM **9g** for 24 h at 37 °C. (c) Incubation of $A\beta_{1-42}$ with 40 μM **9g** for 24 h at 37 °C. (d) Incubation of $A\beta_{1-42}$ with 20 μM Cu^{2+} and 40 μM **9g** for 24 h at 37 °C. (e) Incubation of $A\beta_{1-42}$ with 20 μM Fe^{2+} and 40 μM **9g** for 24 h at 37 °C. (f) Incubation of $A\beta_{1-42}$ with 20 μM Cu^{2+} for 24 h at 37 °C. (g) Incubation of $A\beta_{1-42}$ with 20 μM Fe^{2+} for 24 h at 37 °C.

ability of **9g** to inhibit ChE in the presence of metal ions and $A\beta_{1-42}$ was examined by following a procedure reported previously [61]. As shown in Table 2, **9g** showed good inhibition to both AChE and BuChE, with IC_{50} values of 796 nM and 495 nM for AChE and BuChE respectively in HEPES buffer (pH 6.6, Condition a). The presence of metal ions or $A\beta_{1-42}$ (Conditions b–d) had little effect to the inhibitory activity of **9g** to ChE. Compound **9g** retained good inhibition to ChE in the presence of metal ions or $A\beta_{1-42}$, indicating that inhibition of ChE by compound **9g** is not influenced by its Aβ disaggregation and anti-oxidation activity for Alzheimer's disease and the multifunctional effects of **9g**.

3.13. Dot plot, gel electrophoresis and Western blot analysis for the inhibition of $A\beta_{1-42}$ aggregation by 9g

The inhibition of $A\beta_{1-42}$ aggregation by **9g** was further analyzed by using dot plot, gel electrophoresis, and Western Blotting. Dot-blot assays of the Aβ samples were performed using Aβ fibril-specific antibody B10 [62], which preferentially recognizes amyloid fibrils but does not bind to monomers or small oligomers. The antibody used in the gel electrophoresis was 6E10. As shown in Fig. 7, Cu^{2+} and Fe^{2+} could accelerate the formation of $A\beta_{1-42}$, which is consistent with our ThT result. The incubation of $A\beta_{1-42}$ with **9g** reduced Aβ fibril formation, as indicated by B10 immunoreactivity. Our results showed that **9g** could reduce both Aβ self-aggregation and metal-induced Aβ-aggregation. Besides, as shown in Fig. 8b and c, more lower molecular weight (≤25 kDa) Aβ species were visualized by using native gel electrophoresis followed by Western blot with 6E10. Compound **9g** had dose-dependent inhibition of Aβ fibril formation, and stabilized lower molecular weight Aβ species. For Cu^{2+}-induced (Fig. 8f) and Fe^{2+}-induced (Fig. 8g) Aβ-aggregation, more lower molecular weight Aβ species could be observed upon incubation with **9g** (Fig. 8d and e), indicating that **9g** could reduce metal-induced Aβ-aggregation.

3.14. Effect of 9g on Aβ β-sheet formation

It has been known that Aβ adopt a conformational mixture of α-helix, β-sheet, and random coil in aqueous solution, and undergo a conformational change to form intramolecular β-sheet structure in the fibrillization [63]. These β-sheets have been suggested of contributing to the toxicity of Aβ [64]. In order to further investigate the mechanism of **9g**-induced Aβ conformational transformation, CD spectroscopy was used to monitor the change of $A\beta_{1-42}$ secondary structure during the assembly stage without or with different concentrations of **9g**. As shown in Fig. 9, freshly prepared $A\beta_{1-42}$ in phosphate buffer solution had no obvious α-helix and β-sheet (Fig. 9A), which indicates unfolded peptide structure. After 48 h of incubation at 37 °C, a maximal positive absorbance around 195 nm (the general characteristic of α-helix) and a negative absorbance around 218 nm (the general characteristic of β-sheets) were observed (Fig. 9b). The addition of **9g** decreased the absorbance at both 195 nm and 218 nm. Thus, **9g** could stabilize random $A\beta_{1-42}$ and reduce the formation of α-helix and β-sheet structure of the peptide, which could partially explain its inhibition of Aβ aggregation.

3.15. Molecular modeling study for the binding mode of 9g with AChE and BuChE as well as $A\beta_{1-42}$

To investigate the binding modes between compound **9g** and AChE, BuChE, as well as Aβ, molecular docking studies were carried out. As shown in Fig. 10A, compound **9g** could well occupy the PAS of AChE and forms hydrophobic interactions with residues Phe297, Phe295, Leu289, Val294, Trp286, Tyr337, Phe338, Tyr341, and Trp86. The introduction of pyridine moiety at the end of chain can enhance AChE inhibition activity because it can form π–π stacking interactions with Tyr336 and Trp86 (Fig. 10B). Compared the binding modes of compound **9g** with ligand F11 (a known inhibitor occupies two binding sites of

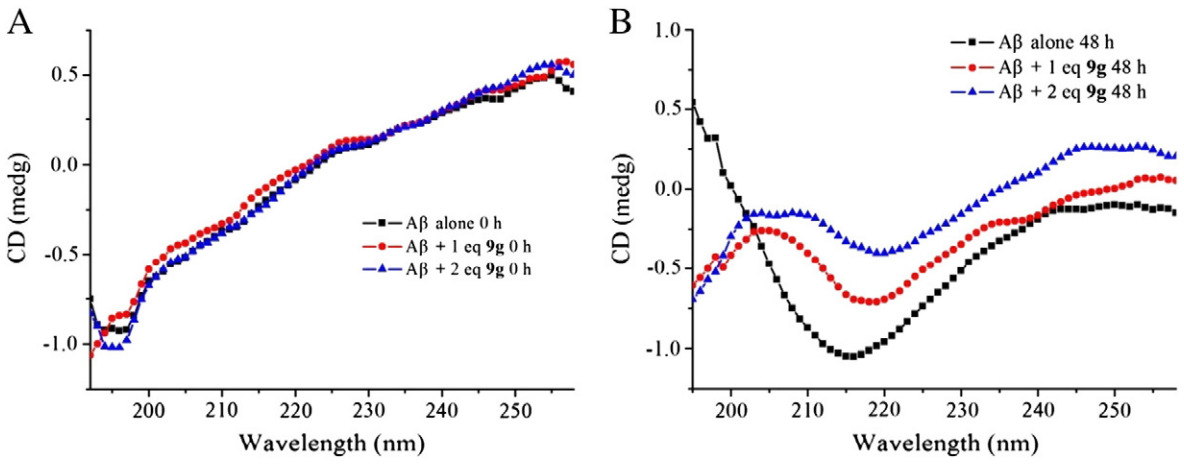

Fig. 9. (A) CD spectroscopy for incubation of $A\beta_{1-42}$ alone (20 μM) and $A\beta_{1-42}$ with compound **9g** (20 μM, 40 μM) at 37 °C for 0 h. (B) CD spectroscopy for incubation of $A\beta_{1-42}$ alone (20 μM) and $A\beta_{1-42}$ with compound **9g** (20 μM, 40 μM) at 37 °C for 48 h.

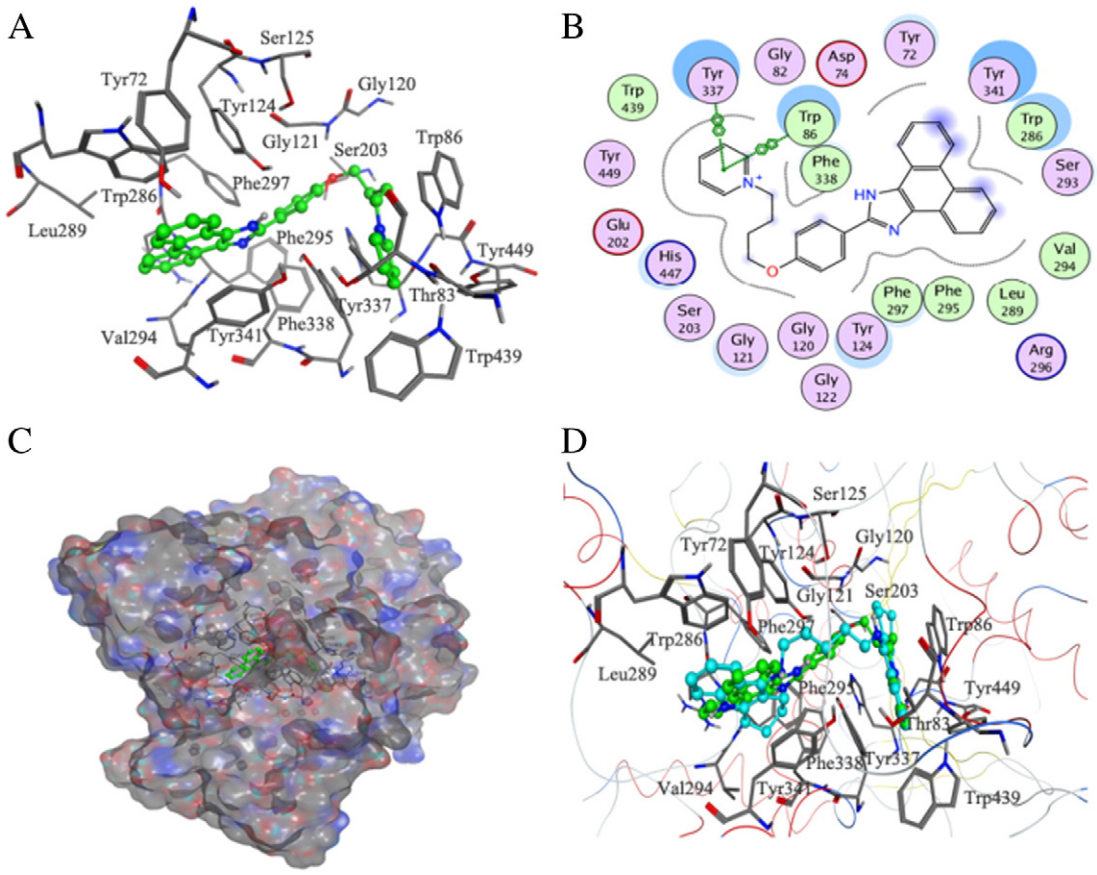

Fig. 10. Binding mode for **9g**–AChE complex. (A) 3D ligand-interaction diagram. (B) 2D ligand-interaction diagram. (C) The polar and hydrophobic surface profile of human AChE with compound **9g**. (D) Superposition of **9g** with F11 in ligand-binding pocket. Blue carbon represents compound **9g** and cyan carbon represents compound F11.

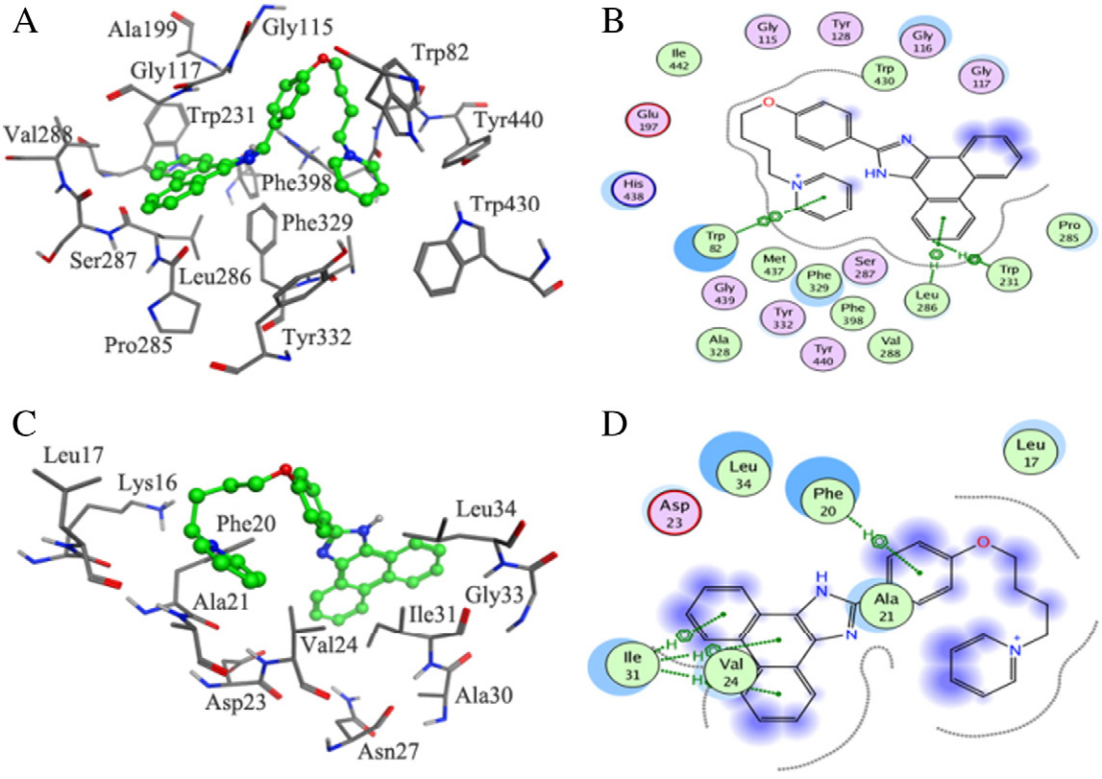

Fig. 11. Binding modes for **9g**–BuChE and **9g**–Aβ_{1-42} complexes. (A) 3D ligand-interaction diagram of **9g**–BuChE. (B) 2D ligand-interaction diagram of **9g**–BuChE. (C) 3D ligand-interaction diagram of **9g**–Aβ_{1-42}. (D) 2D ligand-interaction diagram of **9g**–Aβ_{1-42}.

AChE), the binding mode of **9g** with AChE was similar to that of the ligand F11 (Fig. 10D), suggesting its dual binding mode and mixed type inhibition of AChE. These results are consistent with our biological assay results. In addition, the binding mode of **9g** with BuChE was also investigated. As shown in Fig. 11A and B, compound **9g** binds to the catalytic site of BuChE. The 1H-phenanthro[9,10-d]imidazole structure of **9g** forms H–π interactions with Trp231 and Leu286, while the pyridine moiety of **9g** forms the H–π interaction with residue Trp82. Like compound **9g** against AChE, the hydrophobic interactions are favourable to the inhibitory effect of **9g** for BuChE, which is consistent with our bioassay results.

Previous studies have suggested that the formation of the β-sheet structure in Aβ can promote the aggregation of Aβ [65], and molecules binding to *C*-terminus of Aβ could decrease the formation of β-sheet so as to inhibit Aβ aggregation [66,67]. The binding mode of **9g** with $A\beta_{1-42}$ was studied based on previous docking method [58]. As shown in Fig. 11C and D, compound **9g** binds to the *C*-terminus of $A\beta_{1-42}$ and is stabilized by hydrophobic interactions. **9g** can form H–π stacking interactions with Ile31 and Phe20, and the expanded aromatic structure of **9g** facilitates the formation of its hydrophobic interactions with Ile31, Val24, Ala21, Phe20, and Leu34. The *C*-terminus binding mode and the hydrophobic interactions may explain the mechanism for the disaggregation of $A\beta_{1-42}$ by **9g**, which is also consistent with our CD results. Our above analyses rationalized our experimental result, which indicated that compound **9g** could be a multifunctional agent for the treatment of AD.

Funding

This work was supported by the National Natural Science Foundation of China (Grants 21242010, 81273433, and 81001372), Research Fund for the Doctoral Program of Higher Education of China (Grant 20110171110051), and the National High Technology Research and Development Program of China (863 Program) (Grant 2012AA020307).

Appendix A. Supplementary data

Supplementary data to this article can be found online at http://dx.doi.org/10.1016/j.bbagen.2014.05.005.

References

[1] K. Blennow, M.J. de Leon, H. Zetterberg, Alzheimer's disease, Lancet 368 (2006) 387–403.
[2] V.H. Finder, Alzheimer's disease: a general introduction and pathomechanism, J. Alzheimers Dis. 22 (Suppl. 3) (2010) 5–19.
[3] R.E. Tanzi, L. Bertram, Twenty years of the Alzheimer's disease amyloid hypothesis: a genetic perspective, Cell 120 (2005) 545–555.
[4] A. Abbott, Dementia: a problem for our age, Nature 475 (2011) S2–S4.
[5] E.D. Roberson, L. Mucke, 100 years and counting: prospects for defeating Alzheimer's disease, Science 314 (2006) 781–784.
[6] P.A. Adlard, S.A. James, A.I. Bush, C.L. Masters, beta-Amyloid as a molecular therapeutic target in Alzheimer's disease, Drugs Today 45 (2009) 293–304.
[7] M. Citron, Alzheimer's disease: strategies for disease modification, Nat. Rev. Drug Discov. 9 (2010) 387–398.
[8] D.J. Selkoe, Resolving controversies on the path to Alzheimer's therapeutics, Nat. Med. 17 (2011) 1060–1065.
[9] A. Abbott, Neuroscience: The plaque plan, Nature 456 (2008) 161–164.
[10] J. Hardy, D.J. Selkoe, The amyloid hypothesis of Alzheimer's disease: progress and problems on the road to therapeutics, Science 297 (2002) 353–356.
[11] A.S. DeToma, S. Salamekh, A. Ramamoorthy, M.H. Lim, Misfolded proteins in Alzheimer's disease and type II diabetes, Chem. Soc. Rev. 41 (2012) 608–621.
[12] L.E. Scott, C. Orvig, Medicinal inorganic chemistry approaches to passivation and removal of aberrant metal ions in disease, Chem. Rev. 109 (2009) 4885–4910.
[13] D.J. Selkoe, Cell biology of protein misfolding: the examples of Alzheimer's and Parkinson's diseases, Nat. Cell Biol. 6 (2004) 1054–1061.
[14] P.J. Crouch, S.-M.E. Harding, A.R. White, J. Camakaris, A.I. Bush, C.L. Masters, Mechanisms of Aβ mediated neurodegeneration in Alzheimer's disease, Int. J. Biochem. Cell Biol. 40 (2008) 181–198.
[15] A. Rauk, The chemistry of Alzheimer's disease, Chem. Soc. Rev. 38 (2009) 2698–2715.
[16] K.P. Kepp, Bioinorganic chemistry of Alzheimer's disease, Chem. Rev. 112 (2012) 5193–5239.
[17] R. Jakob-Roetne, H. Jacobsen, Alzheimer's disease: from pathology to therapeutic approaches, Angew. Chem. Int. Ed. 48 (2009) 3030–3059.
[18] P.J. Crouch, K.J. Barnham, Therapeutic redistribution of metal ions to treat Alzheimer's disease, Acc. Chem. Res. 45 (2012) 1604–1611.
[19] A.S. Pithadia, M.H. Lim, Metal-associated amyloid-β species in Alzheimer's disease, Curr. Opin. Chem. Biol. 16 (2012) 67–73.
[20] A.I. Bush, R.E. Tanzi, Therapeutics for Alzheimer's disease based on the metal hypothesis, Neurotherapeutics 5 (2008) 421–432.
[21] J. Pierre, M. Fontecave, Iron and activated oxygen species in biology: the basic chemistry, Biometals 12 (1999) 195–199.
[22] X. Zhu, B. Su, X. Wang, M.A. Smith, G. Perry, Causes of oxidative stress in Alzheimer disease, Cell. Mol. Life Sci. 64 (2007) 2202–2210.
[23] P. Zatta, D. Drago, S. Bolognin, S.L. Sensi, Alzheimer's disease, metal ions and metal homeostatic therapy, Trends Pharmacol. Sci. 30 (2009) 346–355.
[24] Y. Chen, J. Sun, L. Fang, M. Liu, S. Peng, H. Liao, J. Lehmann, Y. Zhang, Tacrine-ferulic acid-nitric oxide (NO) donor trihybrids as potent, multifunctional acetyl- and butyrylcholinesterase inhibitors, J. Med. Chem. 55 (2012) 4309–4321.
[25] M. Harel, L.K. Sonoda, I. Silman, J.L. Sussman, T.L. Rosenberry, Crystal structure of thioflavin T bound to the peripheral site of *Torpedo californica* acetylcholinesterase reveals how thioflavin T acts as a sensitive fluorescent reporter of ligand binding to the acylation site, J. Am. Chem. Soc. 130 (2008) 7856–7861.
[26] A.E. Reyes, M.A. Chacón, M.C. Dinamarca, W. Cerpa, C. Morgan, N.C. Inestrosa, Acetylcholinesterase–Aβ complexes are more toxic than Aβ fibrils in rat hippocampus: effect on rat β-Amyloid aggregation, laminin expression, reactive astrocytosis, and neuronal cell loss, Am. J. Pathol. 164 (2004) 2163–2174.
[27] M. Rosini, V. Andrisano, M. Bartolini, M.L. Bolognesi, P. Hrelia, A. Minarini, A. Tarozzi, C. Melchiorre, Rational approach to discover multipotent anti-Alzheimer drugs, J. Med. Chem. 48 (2005) 360–363.
[28] M.I. Fernandez-Bachiller, C. Perez, G.C. Gonzalez-Munoz, S. Conde, M.G. Lopez, M. Villarroya, A.G. Garcia, M.I. Rodriguez-Franco, Novel tacrine-8-hydroxyquinoline hybrids as multifunctional agents for the treatment of Alzheimer's disease, with neuroprotective, cholinergic, antioxidant, and copper-complexing properties, J. Med. Chem. 53 (2010) 4927–4937.
[29] A. Cavalli, M.L. Bolognesi, S. Capsoni, V. Andrisano, M. Bartolini, E. Margotti, A. Cattaneo, M. Recanatini, C. Melchiorre, A small molecule targeting the multifactorial nature of Alzheimer's disease, Angew. Chem. Int. Ed. 46 (2007) 3689–3692.
[30] M.L. Bolognesi, R. Banzi, M. Bartolini, A. Cavalli, A. Tarozzi, V. Andrisano, A. Minarini, M. Rosini, V. Tumiatti, C. Bergamini, R. Fato, G. Lenaz, P. Hrelia, A. Cattaneo, M. Recanatini, C. Melchiorre, Novel class of quinone-bearing polyamines as multi-target-directed ligands to combat Alzheimer's disease, J. Med. Chem. 50 (2007) 4882–4897.
[31] S. Noel, S. Cadet, E. Gras, C. Hureau, The benzazole scaffold: a SWAT to combat Alzheimer's disease, Chem. Soc. Rev. 42 (2013) 7747–7762.
[32] A.S. Alpan, S. Parlar, L. Carlino, A.H. Tarikogullari, V. Alptuzun, H.S. Gunes, Synthesis, biological activity and molecular modeling studies on 1H-benzimidazole derivatives as acetylcholinesterase inhibitors, Bioorg. Med. Chem. 21 (2013) 4928–4937.
[33] J. Zhu, C.F. Wu, X. Li, G.S. Wu, S. Xie, Q.N. Hu, Z. Deng, M.X. Zhu, H.R. Luo, X. Hong, Synthesis, biological evaluation and molecular modeling of substituted 2-aminobenzimidazoles as novel inhibitors of acetylcholinesterase and butyrylcholinesterase, Bioorg. Med. Chem. 21 (2013) 4218–4224.
[34] M. Ouberai, P. Dumy, S. Chierici, J. Garcia, Synthesis and biological evaluation of clicked curcumin and clicked KLVFFA conjugates as inhibitors of β-amyloid fibril formation, Bioconjug. Chem. 20 (2009) 2123–2132.
[35] C.M. Peter, J.M. Roeland, Synthesis and single enzyme activity of a clicked lipase-BSA hetero-dimer, Chem. Commun. (2006) 2012–2014.
[36] J. Bieschke, M. Herbst, T. Wiglenda, R.P. Friedrich, A. Boeddrich, F. Schiele, D. Kleckers, J.M.L. del Amo, B.A. Grüning, Q. Wang, Small-molecule conversion of toxic oligomers to nontoxic β-sheet-rich amyloid fibrils, Nat. Chem. Biol. 8 (2011) 93–101.
[37] A.K. Sharma, S.T. Pavlova, J. Kim, D. Finkelstein, N.J. Hawco, N.P. Rath, J. Kim, L.M. Mirica, Bifunctional compounds for controlling metal-mediated aggregation of the Aβ42 peptide, J. Am. Chem. Soc. 134 (2012) 6625–6636.
[38] S.-Y. Chen, Y. Chen, Y.-P. Li, S.-H. Chen, J.-H. Tan, T.-M. Ou, L.-Q. Gu, Z.-S. Huang, Design, synthesis, and biological evaluation of curcumin analogues as multifunctional agents for the treatment of Alzheimer's disease, Bioorg. Med. Chem. 19 (2011) 5596–5604.
[39] E.H. Rydberg, B. Brumshtein, H.M. Greenblatt, D.M. Wong, D. Shaya, L.D. Williams, P.R. Carlier, Y.-P. Pang, I. Silman, J.L. Sussman, Complexes of alkylene-linked tacrine dimers with torpedo californica acetylcholinesterase: binding of bis(5)-tacrine produces a dramatic rearrangement in the active-site gorge, J. Med. Chem. 49 (2006) 5491–5500.
[40] Schrödinger Suite, Schrödinger, LLC, New York, NY, 2013.
[41] A. Cheng, S.A. Best, K.M. Merz Jr., C.H. Reynolds, GB/SA water model for the Merck molecular force field (MMFF), J. Mol. Graph. Model. 18 (2000) 273–282.
[42] Y. Nicolet, O. Lockridge, P. Masson, J.C. Fontecilla-Camps, F. Nachon, Crystal structure of human butyrylcholinesterase and of its complexes with substrate and products, J. Biol. Chem. 278 (2003) 41141–41147.
[43] O. Crescenzi, S. Tomaselli, R. Guerrini, S. Salvadori, A.M. D'Ursi, P.A. Temussi, D. Picone, Solution structure of the Alzheimer amyloid β-peptide (1–42) in an apolar microenvironment, Eur. J. Biochem. 269 (2002) 5642–5648.
[44] G.M. Morris, R. Huey, W. Lindstrom, M.F. Sanner, R.K. Belew, D.S. Goodsell, A.J. Olson, AutoDock4 and AutoDockTools4: automated docking with selective receptor flexibility, J. Comput. Chem. 30 (2009) 2785–2791.

[45] W.C. Drewe, S. Neidle, Click chemistry assembly of G-quadruplex ligands incorporating a diarylurea scaffold and triazole linkers, Chem. Commun. (2008) 5295–5297.
[46] J.E. Moses, D.J. Ritson, F. Zhang, C.M. Lombardo, S. Haider, N. Oldham, S. Neidle, A click chemistry approach to C3 symmetric, G-quadruplex stabilising ligands, Org. Biomol. Chem. 8 (2010) 2926–2930.
[47] A.D. Moorhouse, A.M. Santos, M. Gunaratnam, M. Moore, S. Neidle, J.E. Moses, Stabilization of G-quadruplex DNA by highly selective ligands via click chemistry, J. Am. Chem. Soc. 128 (2006) 15972–15973.
[48] H.C. Kolb, M. Finn, K.B. Sharpless, Click chemistry: diverse chemical function from a few good reactions, Angew. Chem. Int. Ed. 40 (2001) 2004–2021.
[49] M. Bartolini, C. Bertucci, M.L. Bolognesi, A. Cavalli, C. Melchiorre, V. Andrisano, Insight into the kinetic of Amyloid β (1–42) peptide self-aggregation: elucidation of inhibitors' mechanism of action, ChemBioChem 8 (2007) 2152–2161.
[50] G.L. Ellman, K.D. Courtney, V. Andres jr., R.M. Featherstone, A new and rapid colorimetric determination of acetylcholinesterase activity, Biochem. Pharmacol. 7 (1961) 88–95.
[51] A. Dávalos, C. Gómez-Cordovés, B. Bartolomé, Extending applicability of the oxygen radical absorbance capacity (ORAC–Fluorescein) assay, J. Agric. Food Chem. 52 (2003) 48–54.
[52] B. Ou, M. Hampsch-Woodill, R.L. Prior, Development and validation of an improved oxygen radical absorbance capacity assay using fluorescein as the fluorescent probe, J. Agric. Food Chem. 49 (2001) 4619–4626.
[53] J.-S. Choi, J.J. Braymer, R.P. Nanga, A. Ramamoorthy, M.H. Lim, Design of small molecules that target metal-Aβ species and regulate metal-induced Aβ aggregation and neurotoxicity, Proc. Natl. Acad. Sci. 107 (2010) 21990–21995.
[54] C. Lu, Y. Guo, J. Yan, Z. Luo, H.-B. Luo, M. Yan, L. Huang, X. Li, Design, synthesis, and evaluation of multitarget-directed resveratrol derivatives for the treatment of alzheimer's disease, J. Med. Chem. 56 (2013) 5843–5859.
[55] J. Geng, M. Li, L. Wu, J. Ren, X. Qu, Liberation of copper from Amyloid plaques: making a risk factor useful for Alzheimer's disease treatment, J. Med. Chem. 55 (2012) 9146–9155.
[56] Y. Oyama, A. Hayashi, T. Ueha, K. Maekawa, Characterization of 2′,7′-dichlorofluorescin fluorescence in dissociated mammalian brain neurons: estimation on intracellular content of hydrogen peroxide, Brain Res. 635 (1994) 113–117.
[57] P. Riederer, W. Danielczyk, E. Grünblatt, Monoamine oxidase-B inhibition in Alzheimer's disease, NeuroToxicology 25 (2004) 271–277.
[58] Y.Y. Cao, L. Wang, H. Ge, X.L. Lu, Z. Pei, Q. Gu, J. Xu, Salvianolic acid A, a polyphenolic derivative from *Salvia miltiorrhiza* bunge, as a multifunctional agent for the treatment of Alzheimer's disease, Mol. Divers. (2013) 1–10.
[59] M.L. Bolognesi, A. Cavalli, C. Melchiorre, Memoquin: a multi-target-directed ligand as an innovative therapeutic opportunity for Alzheimer's disease, Neurotherapeutics 6 (2009) 152–162.
[60] M. Bartolini, C. Bertucci, V. Cavrini, V. Andrisano, β-Amyloid aggregation induced by human acetylcholinesterase: inhibition studies, Biochem. Pharmacol. 65 (2003) 407–416.
[61] A. Kochi, T.J. Eckroat, K.D. Green, A.S. Mayhoub, M.H. Lim, S. Garneau-Tsodikova, A novel hybrid of 6-chlorotacrine and metal-amyloid-β modulator for inhibition of acetylcholinesterase and metal-induced amyloid-β aggregation, Chem. Sci. 4 (2013) 4137–4145.
[62] G. Habicht, C. Haupt, R.P. Friedrich, P. Hortschansky, C. Sachse, J. Meinhardt, K. Wieligmann, G.P. Gellermann, M. Brodhun, J. Götz, K.-J. Halbhuber, C. Röcken, U. Horn, M. Fändrich, Directed selection of a conformational antibody domain that prevents mature amyloid fibril formation by stabilizing Aβ protofibrils, Proc. Natl. Acad. Sci. 104 (2007) 19232–19237.
[63] P. Pratim Bose, U. Chatterjee, C. Nerelius, T. Govender, T. Norström, A. Gogoll, A. Sandegren, E. Göthelid, J. Johansson, P.I. Arvidsson, Poly-N-methylated amyloid β-peptide (Aβ) C-terminal fragments reduce Aβ toxicity in vitro and in *Drosophila melanogaster*, J. Med. Chem. 52 (2009) 8002–8009.
[64] A. Lorenzo, B.A. Yankner, Beta-amyloid neurotoxicity requires fibril formation and is inhibited by congo red, Proc. Natl. Acad. Sci. 91 (1994) 12243–12247.
[65] C. Soto, E.M. Castaño, R. Asok Kumar, R.C. Beavis, B. Frangione, Fibrillogenesis of synthetic amyloid-β peptides is dependent on their initial secondary structure, Neurosci. Lett. 200 (1995) 105–108.
[66] S.S.S. Wang, Y.-T. Chen, S.-W. Chou, Inhibition of amyloid fibril formation of β-amyloid peptides via the amphiphilic surfactants, Biochim. Biophys. Acta Mol. Basis Dis. 1741 (2005) 307–313.
[67] A.J. Doig, Peptide inhibitors of beta-amyloid aggregation, Curr. Opin. Drug Discov. 10 (2007) 533–539.